ADVANCED OPTICAL MATERIALS
www.advopticalmat.de

Materials Views
www.MaterialsViews.com

Photoreduction of Graphene Oxides: Methods, Properties, and Applications

Yong-Lai Zhang, Li Guo, Hong Xia, Qi-Dai Chen, Jing Feng, and Hong-Bo Sun**

In view of mass-production and solution-processing capabilities, graphene oxides (GOs), generally prepared by chemical oxidation of graphite and subsequent exfoliation in aqueous solution, are widely used as an effective route to graphene-like materials. However, the oxygen-containing groups (OCGs) on the graphene sheets make GO insulating, which significantly restricts its applications, especially for electronics. Therefore, reduction methods that are used to remove OCGs become critical. In recent years, in addition to thermal and chemical reduction, photoreduction has emerged as an appealing alternative because photoreduction does not rely on either high temperature or toxic chemicals. In this progress report, the recent development of the photoreduction of GOs and their unique properties are highlighted, as well as their related applications. Photoreduction strategies including photothermal reduction, catalytic/catalyst-free photochemical reduction, and solid state/in-solution laser reduction are summarized. Moreover, photoreduction of GO permits exquisite control over film conductivities, residual oxygen contents, porosity, and surface wettability, which lead to various functionalities towards a wide range of applications, such as field-effect-transistors (FETs), flexible electrodes, sensors, supercapacitors, Li-ion batteries, photovoltaic devices, and photocatalysis. It is anticipated that, with the rapid progress of photoreduction methodology, GOs would be more competitive in the graphene-oriented applications.

1. Introduction

Ever since the first discovery of isolated single-atom thick graphite planes by using the "Scotch tape method" in 2004,[1] the unique 2D carbon crystal named graphene has emerged as a rapidly rising star on the horizon of materials science and modern physics.[2] To date, despite a short history, graphene has already revealed a cornucopia of both fundamental research and broad applications.[3–8] As compared with its predecessors, such as graphite and carbon nanotubes, graphene exhibits many exceptional properties, including an ultra-high carrier mobility (200 000 cm^2 V^{-1} S^{-1}),[9,10] optical transmittance (~97.7%, λ = 550 nm),[11] high thermal conductivity (~5000 Wm^{-1} K^{-1}),[12] high Young's modulus (~1.0 TPa),[13] high electrical conductivity,[14] flexibility,[15] high chemical/physical stability,[16] and biocompatibility.[17,18] All of these properties have contributed to its great potential in various applications, for example, field-effect transistors (FETs),[19–22] transparent and flexible electrodes,[23–26] photovoltaics and related devices,[27–31] microsensors,[32–36] optical modulators,[37,38] supercapacitors,[39–41] catalyst supports,[42–44] and even biodevices for tissue engineering.[45–47] However, the problems in the macroscale production of graphene are the main barrier to their practical use, despite the fact that graphene has been readily prepared by several approaches including mechanical exfoliation of graphite,[48,49] epitaxial growth on silicon carbide via silicon sublimation,[50–52] and chemical vapor deposition (CVD) growth from carbon precursors on metal substrates (e.g., Cu, Ni).[27,53–56] Therefore, there is an urgent call for new methodologies which are distinguished by repeatability and can be implemented on the macroscale for the cost-effective production of graphene.

As an alternative, graphene oxides (GOs), prepared by chemical oxidation of graphite and subsequent exfoliation in water, have been recognized as a promising precursor for bulk production of graphene-like materials and devices.[57–66] However, there exist abundant oxygen-containning groups (OCGs, e.g., epoxy, hydroxyl, and carboxyl) on the GO sheet, which make it insulating and significantly restrict its applications, especially in electronics. Therefore, the demands on the methods used for GO reduction become critical. To date, enormous research efforts have been dedicated to the reduction of GO, as evidenced by the vast body of related publications.[61,67–75] In the beginning, methods for GO reduction could be simply categorized into two types, one being chemical reductions and the other thermal treatments.[76–78] Generally, the former approaches make use of a chemical reducing reagent (e.g., hydrazine),[79] whereas the later methods resort to high temperature annealing in inert gases (e.g., >1000 °C).[80] Despite OCGs being effectively removed after reduction treatments, high energy waste with respect

Dr. Y.-L. Zhang, L. Guo, Dr. H. Xia, Prof. Q.-D. Chen, Prof. J. Feng, Prof. H.-B. Sun
State Key Laboratory on Integrated Optoelectronics
College of Electronic Science and Engineering
Jilin University
2699, Qianjin Street, Changchun, 130012, PR China
E-mail: yonglaizhang@jlu.edu.cn; hbsun@jlu.edu.cn
Prof. H.-B. Sun
College of Physics
Jilin University
119 Jiefang Road, Changchun, 130023, PR China

DOI: 10.1002/adom.201300317

to high temperature annealing and the residual contamination derived from chemical reducing agents make these two deoxygenation technologies somewhat unsatisfactory. Moreover, both thermal and chemical reductions suffer from poor compatibility with device fabrication techniques, so alternative methods that do not rely on the use of toxic chemicals or high temperatures become highly desired. Nowhere is this more obvious than in the fabrication and integration of graphene-based devices, where there is a need for exquisite control over the residual oxygen content, conductivity, and even the formation of micropatterns.

As the motivation for the controllable reduction of GO continues to intensify, photoreduction strategies have emerged as appealing alternatives to thermal and chemical methods. In recent years, various photo-induced deoxygenizations of GO (photothermal reduction,[81,82] photochemical reduction,[83–85] and laser reduction[86–88]) have become a very important branch of GO reduction methodology. As compared with conventional thermal and chemical routes, photoreduction of GO shows the distinct advantages of high efficiency, low cost, tunable reduction degree, and flexible patterning. Even more important is the flexibility for the fabrication and integration of graphene-based microdevices. In this progress report, we summarize the recent developments of photoreduction strategies of GO and highlight their unique advantages towards a broad range of applications.

Yong-Lai Zhang received his BS (2004) and PhD (2009) from Jilin University, China. He joined Jilin University in 2010 and is currently an associate professor in the State Key Laboratory on Integrated Optoelectronics, College of Electronic Science and Engineering, Jilin University. In 2011, he was awarded a "Hong Kong Scholar" postdoctoral fellowship. His research interests include laser fabrication, graphene-based microdevices, and lab-on-a-chip systems.

Hong-Bo Sun received his PhD from Jilin University, China, in 1996. He worked as a postdoctoral researcher in University of Tokushima, and as an assistant professor in the Department of Applied Physics, Osaka University, from 1996 to 2005. In 2005, he became a professor (Changjiang Scholar) at Jilin University. His research has been focused on laser micro-nanofabrication and its application in microoptics, micromachines, microfluids, and microsensors.

2. GOs and Photoreduction Strategies

As early as 1859, graphite oxide was obtained by treating graphite with strong oxidizers.[89] Later, in 1957, Hummers and co-workers successfully developed an efficient method for quick preparation of graphite oxide, which is still widely used nowadays, known as the "Hummers' method".[90] Since the carbon atom plan of graphite oxide has been decorated by plenty of OCGs which breaks up the extended 2D π-conjugation, the oxidized layers can be easily exfoliated in water with the help of ultrasonication, forming a single layer of graphite oxide, also called graphene oxide (GO),[91] as shown in **Figure 1**. To date, the detailed structure of GO is still uncertain, because the final structure varies with the synthesis method and degree of oxidation.[73] Chemical composition and geometrical shape of individual GO sheets may be different with each other. Generally, GO could be reduced by removing the OCGs and, thereafter, the conjugated structure could be partially recovered, which provides conductivity. Despite previous studies confirming that residual functional groups and defects dramatically alter the structure and properties of reduced GO with respect to pristine graphene,[92,93] reduction methodologies for GO are still promising due to the advantages of large-scale production of graphene-like materials, tractable processing, and the modulation of electronic properties. In this regards, the reduction of GO is of great importance to the development of graphene-based devices fabricated from GO.[25,94–99]

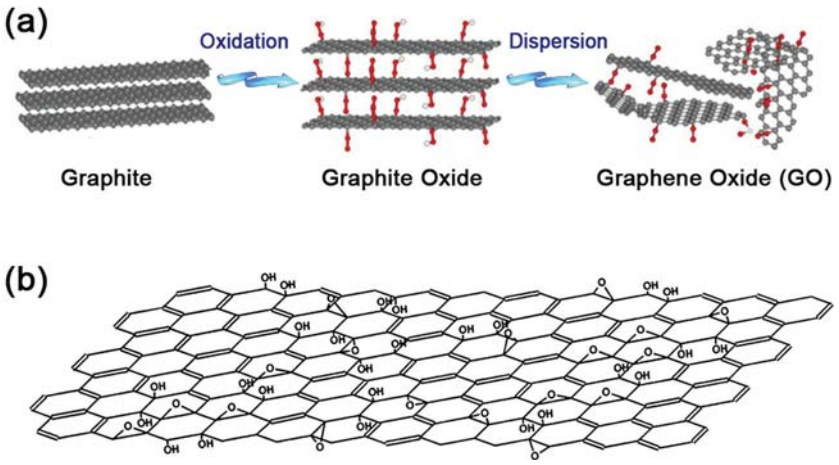

Figure 1. a) Schematic illustration of the preparation of GO from graphite; b) Schematic illustration of the structural model of a GO sheet. Reproduced with permission.[91] Copyright 1998, Elsevier.

Table 1. Typical strategies for solid-state photoreduction of GO and their properties.

Light sources	Atmosphere	Mechanism[a)]	Reduction degree	Conductivity or resistivity[b)]	Ref
Extreme-UV laser (46.9 nm)	–	PC	C–O: 20% decrease	–	[130]
Excimer laser (248 nm)	Vacuum, N_2	PT & PC	C/O: 40	~100–500 Ω/sq	[132]
Excimer pulsed laser (248 nm)	Vacuum	PT & PC	C–C (%): 84	–	[152]
Nd:YAG laser (355 nm)	Air	PT & PC	C/O: 16.9	–	[151,162]
Diode laser (532 nm) Nd:YAG laser (532, 355 nm)	Air, N_2	PT & PC	-	–	[86]
Diode laser (532 nm)	Air	PT & Thermal	C–C (%): 69.2	3830 S/m	[125]
Diode laser (663 nm)	N_2	PT	–	1.1 S/m	[88]
Infrared laser (788 nm)	Air	PT	C/O: 27.8	1650 S/m	[126,127]
Femtosecond laser (790 nm)	Air	PT & PC	C–C (%): 83	2.56×10^4 S/m	[87]
Picosecond laser (1064 nm)	N_2	PT	–	–	[131]
High-pressure Hg lamp (500 W)	H_2 and N_2	PC	C/O: 3.45–5.56	$>10^3$ S/m	[115]
Camera flash (400–800 nm)	Air or N_2	PT	C/O: 4.23	~1000 S/m	[81]
Camera flash	Air	PT	C/O: 11.7	–	[82]
Camera flash	Air	PT	C/O: 15.6	–	[166]
Focused sunlight	Air	PT	C/O: ~33	1500 S/m	[181]
Universal X-660 CO_2 laser	Air	PT	$C_{3.9}O_{2.5}H_{0.9}$	-	[123]

[a)] PT: Photo-thermal reaction; PC: Photo-chemical reaction; [b)] It is not reasonable to compare the conductivities directly, because the film thickness, calculation methods, and the pristine GO samples are different.

Nowadays, the state-of-the-art of the GO reduction methodology can be classified into three categories, thermal reduction, chemical reduction, and photoreduction. Although the former two methods have revealed the strong capability of OCG removal, they are incompatible with device fabrication, especially for that on flexible substrates. By contrast, photoreduction approaches are distinguished due to their moderate reaction conditions, tunable reduction degree, and designable patterning towards device fabrication. In the last five years, photoreduction of GO has been thoroughly investigated. At an early stage, photocatalysts, such as TiO_2, were adopted for reduction of GO through a well-known photochemical process.[69] Later, flash reduction of GO by using a commercial Xenon lamp equipped on a digital camera provided a different mechanism for GO reduction, so-called photothermal reduction.[81] In fact, both photochemical and photothermal reactions are responsible for the removal of OCGs. Smirnov et al. investigated the threshold for GO reduction that requires photon energies lager than 3.2 eV ($\lambda < \approx 390$ nm).[100] According to this threshold argument, catalyst/sensitizer-free photoreduction strategies could be easily categorized into either photochemical or photothermal protocols, excluding those two- or multiphoton absorption processes in laser reduction. In this section, the development of photoreduction of GO is classified into three categories, including photothermal reduction, photochemical reduction, and laser reduction. In fact, laser reductions also undergo either photochemical or photothermal processes, or proceed through a combination of both. The review of laser reductions as a separate section is to emphasize their unique contributions with respect to flexible patterning and device fabrication. To make a clear overview of various photoreduction strategies, the typical methods have been summarized in **Table 1** and **Table 2** for the reduction of GO films and GO solutions, respectively.

2.1. Photothermal Reduction of GO

As compared with conventional chemical and thermal routes, photoreduction has become popular since the first report on flash reduction and patterning of GO by Cote et al.[81] A commercial Xenon lamp equipped on a digital camera was used for the flash reduction of GO and GO/polymer films under ambient conditions. As shown in **Figure 2**a, the dramatic change in color from pristine brown to black indicates the photothermal deoxygenization of GO, which is confirmed by experimental characterization. The method also enables the patterning of GO or GO/polymer films with the help of a photomask. Figure 2b shows the interdigitated reduced graphene oxide (RGO)/polystyrene electrode arrays fabricated on a flexible, 1.5 inch Nylon "wafer". The exposed areas became conductive with the sheet resistance of 9.5 kΩ/square.

Since the camera flash provides mainly visible light ($\lambda > 400$ nm), the removal of OCGs could be attributed to a photothermal effect. To get further insight into the photothermal reduction mechanism, the photoenergy input from the camera flash unit and the thermal energy needed for GO reduction have been calculated.[99] Generally, common camera flash units can deliver 0.1–2 J/cm^2 of energy per pulse at close distances (<2 mm). Taking 1 μm thick GO film as an example, the optical absorption in the visible range (400–800 nm) is ≈63%, accordingly, 63–1260 mJ/m^2 of photoenergy could be deposited on this GO film. However, based on the differential scanning calorimetry (DSC) heating curve of GO, the total

Table 2. Typical photochemical strategies for GO reduction in solution and their properties.

Light sources	Catalysts (stabilizer)	Reduction degree	Conductivity or resistivity	Ref
Excimer laser (248 nm)	(Ammonia)	C–C (%): 94.4	53.8 kΩ/sq	[136]
UV lamp (254 nm, 15 W)	OH–, N_2H_4	O (%): 18 at%	–	[120]
UV light (365 nm, 125 W)	(Polyvinyl pyrrolidone)	–	–	[182]
UV spot lamp (50 W)	–	C/O: 4.5	–	[118]
Medium pressure Hg lamp	(Acrylic resins)	–	–	[183]
High-pressure Hg lamp	$H_3PW_{12}O_{40}$	C–C (%): ≈65.6	–	[108,109]
High-pressure Hg lamp (450 W)	–	C/O: 5.88	–	[184]
High-pressure Hg lamp (500 W)	–	C/O: 3.45–5.56	–	[115]
High-pressure Hg lamp (500 W)	Hantzsch 1,4-dihydropyridine	C–C,C = O (%): ≈77	4680 S/m	[113]
Hg lamp (110 mW/cm^2)	ZnO	–	1.7×10^7Ω/sq	[105]
Hg lamp (200 W)	Electron donors	C–C (%): ≈84	–	[119]
Hg lamp (500 W)	WO_3	–	–	[107]
Hg arc lamp (500 W)	TiO_2	C/O: 14.3	1727 S/m	[101]
Xe lamp (300 W)	–	C/O: 4.23	≈50 S/m	[84]
Xe arc lamp (300 W)	$BiVO_4$	–	–	[106]
Xe lamp (350 W)	TiO_2 & Rhodamine B	C–C (%): 91	–	[103]
Xe lamp (400 W)	Ag, DMF	C–O & C = O (%): 8.1	9000 Ω/sq[a)]	[114]
Xe arc lamp (450 W)	TiO_2	–	–	[69]
Xe lamp (500 W)	–	C/O: 10	–	[117]
Sunlight	Electron donors	–	–	[119]
Incandescent bulb (100 W)	Zinc(II) porphyrin	–	–	[111]
Nd/YAG laser (532, 355 nm)	–	–	–	[133]
532 nm laser	Nanodiamond	–	–	[110]
Femtosecond laser (800 nm)	–	C/O: 8.1	–	[137]

[a)]The resistance of the Ag–RGO film.

thermal energy required to heat the 1 μm thick GO to 100 °C is calculated to be only 70 mJ/cm^2. Considering the fact that deoxygenation of GO occurs even at very low temperature (e.g., ~50 °C), a pulse of camera flash can deliver more than enough energy to trigger the photo-thermal reduction providing most of the absorbed light energy could be converted to heat. Later, Gilje et al. also reported flash reduction of GO foam prepared by freeze-drying GO dispersions.[82] It was discovered that the photothermally initiated deflagration of GO can take place even in an oxygen-deficient environment. The GO foam networks enable greater energy absorption and confinement, leading to dramatic temperature increases (400–500 °C) within a few milliseconds upon exposure to a camera flash.

Photothermal reduction of GO is not limited to a camera flash. In principle, any visible light that can provide enough photoenergy could be used for GO reduction. In the case of photothermal reduction, the light/heat conversion efficiency is the key factor. The use of flash reduction is ingenious, because the pulsed Xenon flash can instantaneously output enough photoenergy to induce deoxygenation, which not only leads to a high efficiency, but also avoids oxygen replenishment. Therefore, a rapid and high degree of reduction of GO can be achieved under ambient conditions. According to Smirnov's threshold effect,[100] the photon energy that can trigger GO reduction should exceed 3.2 eV. In this case, the photothermal effect would commonly exist when the light source used for GO reduction contains a relatively long wavelength range (e.g., > ≈390 nm), for instance, in some laser reductions.[88] To avoid repeated presentation, multiform photoreduction mechanisms that involve photothermal effects are discussed in the following sections.

2.2. Photochemical Reduction of GO

In addition to the photothermal strategies, GO has been reduced through a photochemical scheme, in which the photogenerated electron–hole pairs have been proven to be the general mechanism for the removal of OCGs, leading to the restoration of sp^2 domains. In this section, the methods have been classified into two categories: photocatalytic reduction and direct photochemical reduction.

2.2.1. Photocatalytic Reduction of GO

The earliest work on the photocatalytic reduction of GO was reported by Kamat's group, in 2008.[69] In their study, a mixture of GO and colloidal TiO_2 in ethanol was subjected to steady-state UV irradiation. As shown in **Figure 3**, the electrons from

UV-irradiated TiO_2 suspensions trigger the reduction of GO, which is accompanied by changes in the absorption of the GO, as the color shifts from brown to black. It is well known that semiconducting TiO_2 is a well-researched photocatalyst that has been widely used for the photodegradation of organic contaminants and for the photocatalytic splitting of water. Upon UV irradiation of TiO_2 colloids in the presence of ethanol, the holes are scavenged to produce ethoxy radicals and electrons accumulate within the TiO_2 particles, which serve to interact with the GO sheets to reduce OCGs, as shown in the following equation:

$$TiO_2 + h\upsilon \rightarrow TiO_2(e + h) \quad (1)$$

$$TiO_2(e + h) + C_2H_5OH \rightarrow TiO_2(e) + \bullet C_2H_4OH + H^+ \quad (2)$$

$$TiO_2(e) + GO \rightarrow TiO_2 + rGO \quad (3)$$

Ever since the above-mentioned work, TiO_2 has been widely used for either the photoreduction of GO suspensions or the preparation of RGO/TiO_2 composite materials that could be further used for photocatalysis and dye-sensitized solar cells. For example, Jang et al. reported the photocatalytic synthesis of water-dispersible RGO monosheets without the help of stabilizers or surfactants by separating and recycling the TiO_2.[101] A pure RGO monosheet solution without being bound by TiO_2 was obtained by selective ultracentrifugation separation. After visible-light sensitization of TiO_2 by triethylamine and dyes, visible-light reduction of GO was also reported.[102,103]

It is worthy of note that the irradiation time plays an important role in the controllable removal of OCGs. Generally, an optimum time has to be found for different photoreduction systems. Akhavan et al.[104] found that a prolonged irradiation time would lead to the degradation of RGO. After effective reduction, the carbon content of RGO gradually decreased with increased irradiation time without considerable variation in the reduction level. The photodegradation of RGO was confirmed by Raman spectra and resistivity tests.

The photocatalysts used for GO reduction are not limited to TiO_2. Based on the same idea, ZnO,[105] $BiVO_4$,[106] WO_3,[107] $H_3PW_{12}O_{40}$,[108,109] nanodiamonds,[110] and metalloporphyrin[111,112] have also been used for GO reduction via photocatalytic reactions. In Wu's work, a naturally reduced nicotinamine adenine dinucleotide NAD(P)H model, Hantzsch 1,4-dihydropyridine (HEH), was used as a mild organic photoreductant, for the preparation of "clean" RGO sheets on a large scale.[113] Additionally, Ag nanoparticles have been used as a plasmonic photocatalyst for visible light reduction of GO, in which case, an electron donor is added to promote the reaction.[114]

2.2.2. Direct Irradiation without Photocatalysts

In fact, without the help of any photocatalysts, GO could still be effectively reduced under UV irradiation. For instance, Matsumoto et al.[115] reported the UV reduction of GO under the light from a 500 W high-pressure Hg lamp where ultra pure H_2 or N_2 flowed through a quartz cell. The RGO sheets prepared by this method show significantly reduced OCGs and partially restored sp^2 domains. Moreover, catalyst-free photochemical reduction proceeded even in an aqueous suspension of GO sheets.

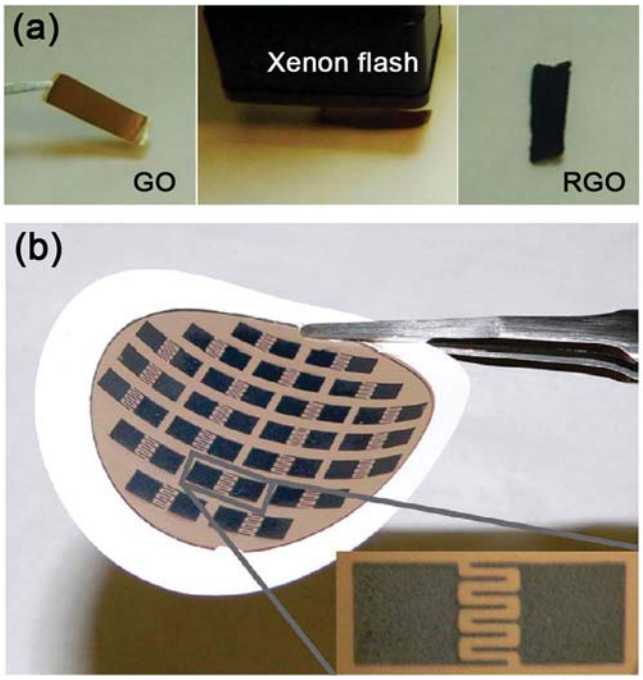

Figure 2. Flash reduction of GO. a) Photographs of GO, flash reduction of GO and RGO, from left to right; b) photograph of the arrays of RGO/polystyrene interdigitated electrodes fabricated on a 1.5 inch diameter GO/polystyrene thin film deposited on a Nylon filter paper. The inset shows the close up view of one set of such electrode. Reproduced with permission.[81] Copyright 2008, American Chemical Society.

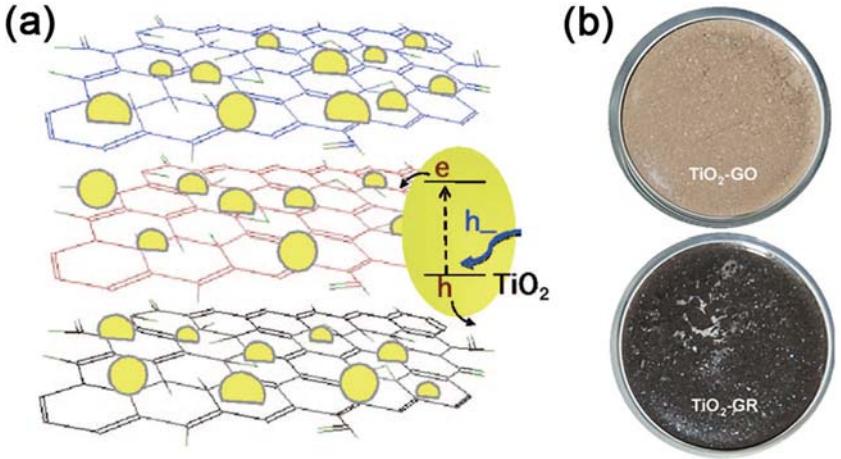

Figure 3. a) Schematic illustration of TiO_2-assisted photoredution of GO under UV excitation; b) photographs of TiO_2–GO composite before and after reduction. Reproduced with permission.[69] Copyright 2008, American Chemical Society.

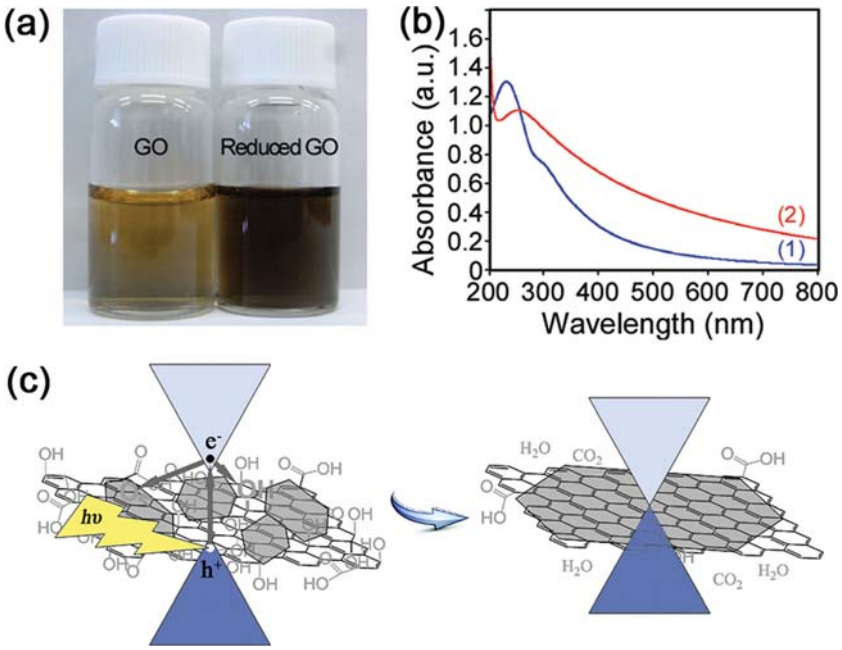

Figure 4. a) Photographs of GO and RGO solution; b) UV–vis spectra of nanosheet suspensions of (1) GO and (2) RGO prepared by photoreduction in H_2 for 2 h. Reproduced with permission.[115] Copyright 2010, American Chemical Society. c) Schematic illustration of the photochemical reduction mechanism of GO to RGO. Reproduced with permission.[84] Copyright 2012, John Wiley and Sons.

As shown in **Figure 4**a,b, the color of the suspension changed from light brown to black after UV irradiation, which could be attributed to the restoration of an $sp^2\pi$-conjugated network.[116] Later, the same research group reported photoreactions similar to photocatalytic reactions in which H_2 and CO_2 are evolved from an aqueous GO suspension under UV irradiation. It was proposed that the semiconducting domains of GO can act as photocatalysts when irradiated with light of energy exceeding the bandgap of the domains.[117]

Recently, Guardia et al. also confirmed the direct reduction of a GO suspension under UV irradiation.[118] Without any photocatalysts, the direct UV irradiation-induced reduction of GO has been considered a self-photocatalytic reduction (SPCR). Sun's group[119] reported the SPCR of a GO suspension in the presence of *N*,*N*-dimethylformamide (DMF), serving as an electron donor. In their work, the use of natural sunlight for such an SPCR reaction was also demonstrated. Motivated by interest in SPCR, Ji et al. investigated the formation and reduction mechanism of UV-reduced GO.[120] GO suspensions in H_2O_2, NaOH, and N_2H_4 solution were exposed to UV irradiation; experimental results showed that the UV-induced $HO^{\cdot}$ radicals from H_2O_2 molecules cannot reduce GO, whereas the existence of OH^- ions or N_2H_4 can promote GO reduction due to the photoinduced electrons on the GO sheets.

Besides UV light, Li et al.[84] reported the photochemical reduction of a GO suspension under visible light towards the green preparation of monolayer graphene sheets. In spite of a certain amount of carboxyl groups remaining, most of the hydroxyl groups of the GO could be selectively removed through this simple irradiation. The reduction of GO under visible light seems contrary to Smirnov's results, in which the threshold for GO reduction is 3.2 eV (λ < 390 nm).[100] Possible reasons for the visible-light reduction would be the SPCR effect and the introduction of a sacrificial electron donor. The schematic illustration of this process is shown in Figure 4c: the photogenerated hole is taken up by the sacrificial electron donor, and the generated electrons split off OH as H_2O from the substitution sites of GO planes to restore the sp^2 domains. Importantly, when the concentration of the GO suspension is low enough (ca. < 0.28 mg/mL), stable aqueous dispersions of graphene monolayers could be prepared, in which the water adlayers play a very important role in stabilizing the graphene monolayers against aggregation.

2.3. Laser Reduction of GO

Laser irradiation has been adopted for GO reduction due to its unique advantages including reliability, amenability, low cost, and flexible patterning.[121] Since the wavelength of a certain laser is invariable, the photoreaction types for various laser reductions could be deduced according to the threshold effect.[100] In principle, reduction by a laser with a wavelength smaller than 390 nm, for instance an excimer laser (248 nm), would mainly undergo a photochemical process, whereas for lasers with wavelengths larger than 390 nm, the photothermal effect accounts for the reduction of GO. However, considering the fact that two-/multiphoton absorption may occur in the case of some tightly focused ultrafast lasers, and laser-induced thermal relaxation commonly exists, most laser reductions may use both photothermal and photochemical effects. In this section, according to the different laser sources used for GO reduction and the reduction environments, the progress in laser reduction of GO is summarized in three parts.

2.3.1. Continuous-Wave Lasers

Zhou et al. firstly reported a "direct laser writing" (DLW) technique for cutting and reducing multilayer GO films, using a continuous wave diode laser (663 nm, 80 mW).[88] **Figure 5** shows the schematic illustration of the DLW treatment of GO films.[122] The cutting of GO films occurs in air when the focused laser beam is incident on a thick multilayer GO film (>5 layers), because the absorbed laser energy is rapidly converted into local heat and raises the local temperature to as high as 500 °C, leading to oxidative decomposition of GO to volatile gases. Instead of oxidative burning, DLW-induced GO reduction has been implemented in an inert atmosphere (N_2). The electrical measurement shows that the laser-reduced region displays an appreciable conductivity of ~1.1 Sm^{-1}. As the laser beam diameter is around 3 μm, simple RGO patterns with feature sizes of approximately 20 μm have been fabricated in a mask-free manner.

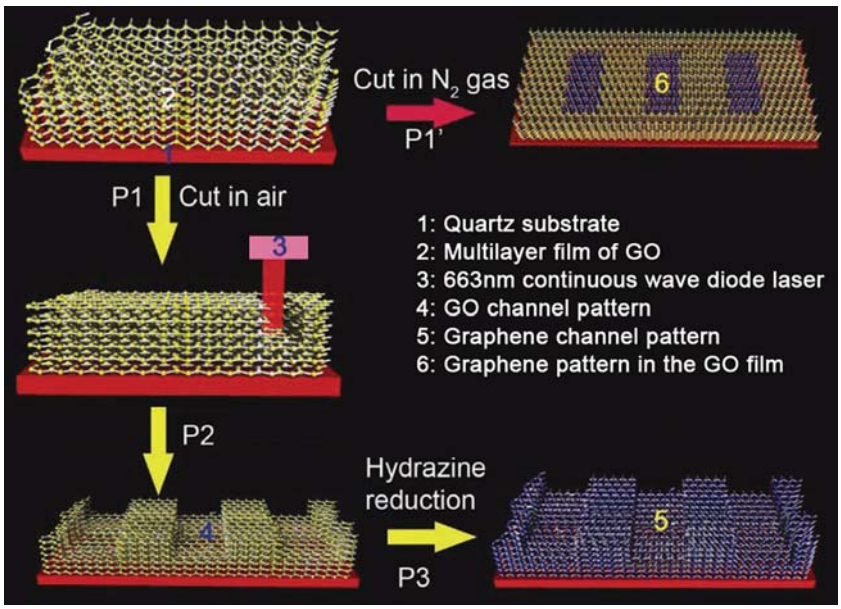

Figure 5. Schematic illustration of the cutting and patterning of GO nanosheets by a focused laser beam. For simplicity of the illustration, the hydroxyl, ether, and carboxylic groups of GO were omitted, and yellow represents GO and blue represents graphene. Reproduced with permission.[122] Copyright 2010, John Wiley and Sons.

Using a similar DLW technique, Gao et al. subsequently demonstrated the laser reduction of GO using a CO_2 laser printer.[123] This was done by scanning a 532 nm continuous-wave diode laser beam over a GO film deposited on SiO_2/Si substrates. Sow's group also reported the reduction and patterning of GO, and conductive strips with a resolution of 1 μm could be created either as channels in the insulating GO matrix, or as a stand-alone microbelt after ultrasonic removal of GO in deionized water.[124] Later, a novel 3D GO–RGO stacked-layered structure with defined micropattern in each layer was developed by the same group. Selective ultrasonic removal of RGO or GO was realized through precise control over the laser power and temperature of the substrate.[125] This was the first report on the 3D patterning of GO or RGO with multilayered structures, which offers more opportunity for the fabrication of complex graphene-based devices.

LightScribe technology, created by the Hewlett-Packard Company, has been widely used to produce laser-etched labels with text and even greyscale graphics, as opposed to stick-on labels and printable discs. Using this facile patterning technique, Kaner's group successfully developed a flexible GO patterning and reduction method towards all-graphene devices.[126] The 788 nm infrared laser of a standard LightScribe DVD optical drive could used reduce GO and even make greyscale RGO graphics. **Figure 6** shows the schematic illustration of the laser-scribing process.[127] A GO film supported on a flexible substrate was firstly covered on a LightScribe-enabled DVD media disc; then the GO film was irradiated by a laser in a computerized LightScribe DVD drive according to predesigned patterns. The low-power infrared laser not only removed most of the OCGs on the GO sheets, rendering its conductivity as high as 1738 S/m, but also transformed the stacked GO sheets into porous structures that endowed it with a high surface area of 1520 m^2/g. This laser scribing technique holds great promise for the development of low-cost graphene-based electronics.

2.3.2. Pulsed Lasers

In addition to continuous wave lasers, ultrafast pulse lasers have also been applied for GO reduction. As early as the beginning of 2010, Zhang et al. reported the direct imprinting of graphene microcircuits by femtosecond laser direct writing (FsLDW)-induced reduction of GO under ambient conditions.[87] In their work, a 790 nm femtosecond laser pulse with a width of 120 fs was focused by a 100× objective lens with a high numerical aperture (NA = 1.4), and a 600 μs exposure

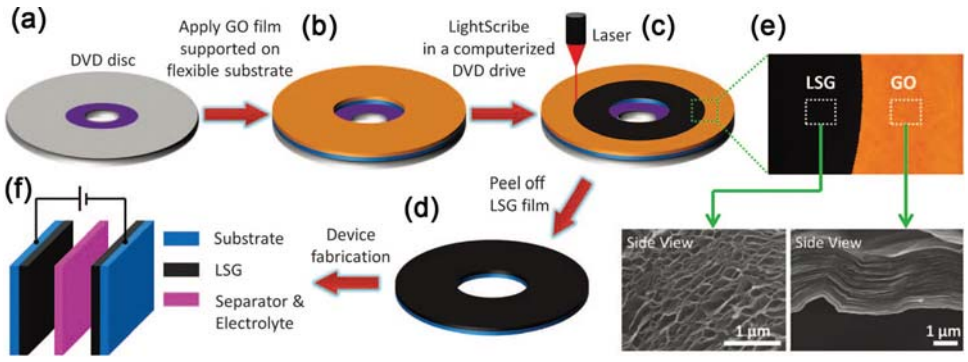

Figure 6. Schematic illustration of the fabrication of laser-scribed RGO electrochemical capacitors. a–d) A GO film supported on a flexible substrate is placed on top of a LightScribe-enabled DVD media disc, and a computer image is then laser-irradiated on the GO film in a computerized LightScribe DVD drive. e) The GO film changes from golden brown to black as it is reduced to RGO. The low-power infrared laser changes the stacked GO sheets immediately into well-exfoliated few-layered laser scribed graphene film, as shown in the cross-sectional SEM images. f) A symmetric EC is constructed from two identical LSG electrodes, ion-porous separator, and electrolyte. Reproduced with permission.[127] Copyright 2012, American Association for the Advancement of Science.

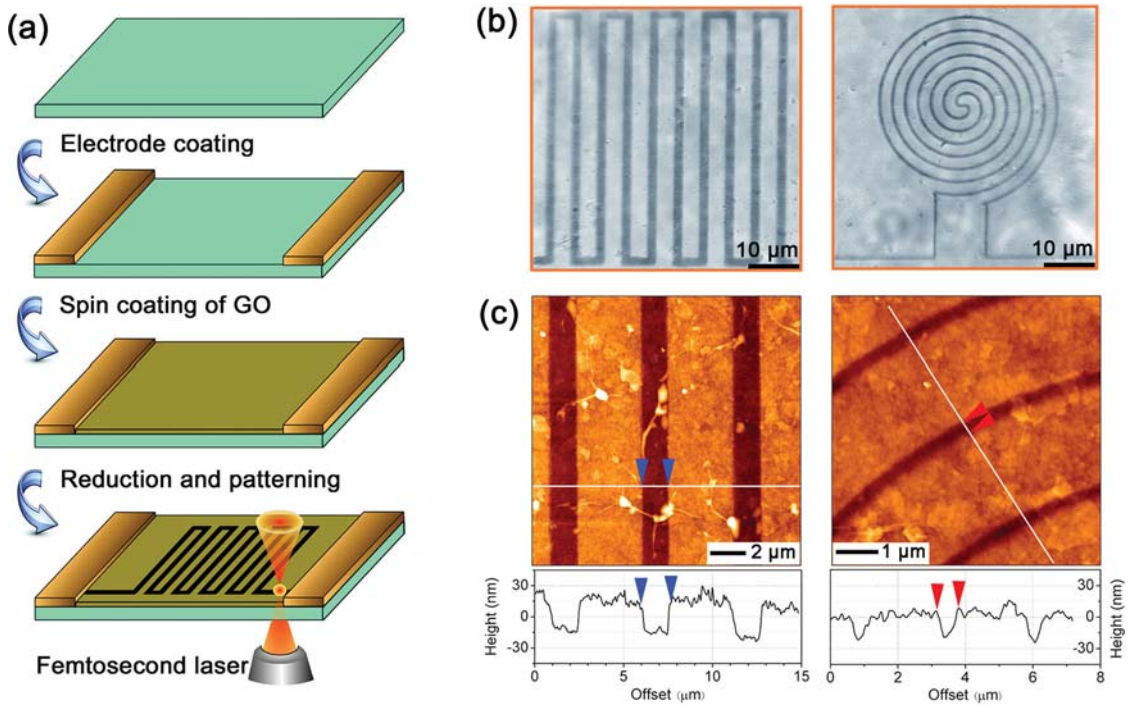

Figure 7. a) Schematic illustration of the FsLDW reduction and patterning of GO; b) optical microscopic images of different micropatterns; c) AFM image of the detail of micropatterns, the bottom two images show the profile of the micropatterns. Reproduced with permission.[87] Copyright 2010, Elsevier.

duration of each voxel and 100 nm scanning step length were adopted for the FsLDW. **Figure 7** shows the schematic illustration of the FsLDW reduction and the as-created micropatterns observed by both optical microscope and atomic force microscope (AFM). Notably, a resolution of 500 nm of the micropatterns could be created by using this technique. The mechanism of this FsLDW-induced deoxygenation could be mainly ascribed to electronic excitation effect and the electron–hole (e–h) recombination-induced thermal effect. During FsLDW, the electronic excitation effect is significant in the first several picoseconds, and this excitation significantly weakens C–O electronic bonding near the top of the valence band, leading to an immediate deoxygenation of GO. After sufficient e–h recombination (i.e., > ≈100 ps), normal heat reduction becomes dominant.

Later, the femtosecond laser irradiation-induced effective reduction of GO was confirmed by performing a first-principles simulation of electron–ion dynamics based on the time-dependent density functional theory.[128] In the simulations, a laser shot was mimicked by an alternating electric field (E field), and electron–ion dynamics were performed for a GO sheet. The simulation, with very short pulse laser width (<5 fs), suggested no significant heating of graphene, and the removal of O atoms from graphene sheets was possible without causing any damage. However, for the experimental results, after femtosecond laser (120 fs pulse width) irradiation, plenty of defects still existed. A possible reason for this phenomenon is the formation of relatively smaller sp^2 domains after laser treatment of the GO film, which could be deduced from the sunken surface of the laser-irradiated region. If a femtosecond laser with a shorter pulse width could be used for GO reduction, damage-free removal of OCGs could be expected; nevertheless, this still needs experimental support.

To evaluate the structural quality of graphene, Raman spectroscopy has been considered one of the most reliable and nondestructive methods. Typically, the G peak at ≈1560 cm^{-1} corresponds to the E_{2g} phonon in the Brillouin zone center, and the D-peak at ≈1360 cm^{-1} is due to the breathing modes of sp^2 atoms and requires a defect for its activation. The 2D peak at ≈2700 cm^{-1} is the second order of the D-peak, which is the most intrinsic to graphene.[129] Sokolov et al. investigated the reduction of GO by using a continuous-wave (CW) Raman microscope 532 nm diode laser in both ambient air and N_2.[86] For comparison, pulsed (≈9 ns, 20 Hz) irradiation of GO using the frequency-doubled (532 nm) and -tripled (355 nm) outputs of a Nd:YAG laser were also carried out. Raman spectra showed the formation of a 2D band and the narrowing of the G band for all the laser reductions, among which GO irradiated with a CW 532 nm beam in N_2 gave the highest reduction degree. In the case of using pulsed lasers, despite significant reduction of GO, the D band feature remained independent of the laser flux, indicating residual defects.

In the pursuit of high-throughput reduction and patterning of GO with nanometer resolution, Prezioso et al. reported a high-throughput resistless extreme-UV (EUV) photolithographic approach operating with sub-micrometer resolution on large-area GO films via spatially resolved photoreduction.[130] Considering the fact that photoreduction of GO is possible at a range of photon energies (i.e., beyond the threshold for photoreduction, ≈3.2 eV, and below the energy threshold that

causes breaking of the in-plane C–C bonds in exfoliated graphene, ≈200–300 eV), that covers the entire EUV range. Therefore EUV light (emitting at $\lambda = 46.9$ nm, 1.5 ns duration, 150 μJ energy) has been adopted for GO reduction through a photochemical mechanism. It is well known that EUV light has for some time been considered the natural candidate to go beyond the resolution limits imposed by UV radiation in standard photolithography, so EUV reduction may hold great promise for making RGO patterns with high resolution.

In addition, the reduction of GO induced by picosecond pulsed laser irradiation has been studied by Trusovas et al.[131] Since the intensity ratio for the D, G, and 2D Raman bands is often used as a criterion of the structural quality of graphene, dependence of the D, G, and 2D Raman band parameters on the laser pulse energy and the irradiation dose has been evaluated. As compared with femtosecond laser pulse, the picosecond laser shows a more obvious thermal effect. According to the modeling of temperature dynamics, a single laser pulse at a fluence of 0.04 J/cm^2 (50 mW) can increase the local temperature of GO by up to 1400 °C for a few nanoseconds, which is sufficient to trigger the reduction of GO. The fully oxidized GO has a strong absorbance at 5.37 eV (231 nm). More recently, to achieve a more efficient optical coupling, 248 nm excimer laser (25 ns pulse width) irradiation of GO in both vacuum and inert N_2 appears to be an effective approach to reduce GO.[132] In Orlando's work, typical sheet resistances of ≈100–500 Ω/sq have been achieved, which is a significant improvement over the values reported in some other laser-mediated GO reductions.

2.3.3. Laser Reduction in Solution

A laser-mediated GO reduction has also been carried out in GO solution. Abdelsayed et al. firstly reported the solution-processable synthesis of individual RGO sheets in water by laser irradiation.[133] The reduction of the GO aqueous solution was carried out under ambient conditions without the use of any chemical reducing agent. Both 532 and 355 nm laser irradiation are capable of reducing GO. Considering the fact that GO solution shows significant absorption below 400 nm and the threshold energy for GO reduction is 3.2 eV, two-photon absorption would probably contribute to the absorption of laser energy by GO in the case of the 532 nm irradiation. However, despite the fact that a nonlinear optical response of GO at 1064 nm has been reported previously,[134] no reduction of GO was observed under 1064 nm irradiation in this work, which is in agreement with the results reported by Feng et al.[135]

Additionally, Huang et al. investigated the reduction of GO in solution using a 248 nm KrF excimer laser.[136] The GO solution in a quartz tube was rapidly reduced after irradiation for only 5 min at room temperature in the presence of ammonia as an inhibitor of RGO aggregation. In addition, a ≈800 nm femtosecond laser has been proven workable for the reduction of GO in aqueous solution without the addition of any reducing agents.[137] Probably, multiphoton absorption occurs in this process. The reduction degree of the resultant GO could be modulated by controlling the irradiation time.

3. Unique Properties of the Photoreduction of GO

Unlike chemical or thermal reduction, the light-mediated reduction of GO can be achieved either through a photochemical process once the photon energy provided by the light source exceeds the threshold (3.2 eV), or through a photothermal mechanism when the light/thermal conversion efficiency is high enough to raise the localized temperature and trigger the deoxidation reaction. Since the energy is provided by a light source, precise control over the wavelength range, intensity, light field distribution, and exposure duration lead to the controllable reduction of GO. Therefore, the photoreduction of GO has unique properties such as mask-free patterning, room-temperature processing, chemical-free and non-contact treatment, controllable reduction, as well as the formation of micro-nanostructures. In this section, we briefly summarized these unique properties in three sections focussing on direct patterning, tunable reduction, and controllable wettability.

3.1. Direct Patterning for Microdevice Fabrication

Rational design and precise patterning of graphene is of considerable importance in the fabrication of graphene-based devices, since they have to be integrated with other functional components in practical applications. For pristine graphene or RGO prepared by chemical/thermal reduction, micropatterns can be readily created through various methods, for instance, by combined techniques involving classical lithography and subsequent O_2 plasma etching.[138,139] In these cases, a pre-patterned protected layer or a shadow mask is necessary for the subsequent etching and the substrates should be very flat. Moreover, the patterning process must have tight contact between the graphene/RGO and the mask layer, which would inevitably cause breakage or contamination of the graphene sheets. In addition, tip techniques have been used for the precise patterning of graphene with ultra-high resolution, even reaching a sub-10 nm level.[140] However, the tip technique usually suffers from low efficiency and is strongly dependent on special instruments.

As an alternative choice, the photoreduction of GO, especially laser reduction, shows the feasibility of making graphene micropatterns in a non-contact manner, revealing a great potential for the fabrication and integration of graphene-based microdevices. As representative examples, Zhang et al. reported the flexible patterning of a GO film by using the FsLDW technique under ambient conditions.[87] The DLW technique is not limited to femtosecond lasers: other laser processing systems such as the use of excimer lasers[132] and continuous-wave CO_2 lasers[123] are also capable of making RGO patterns. Recently, laser scribing induced reduction has showed obvious advantages in the patterning of RGO onto various flexible substrates without masks, templates, post-processing, or transferring techniques.[126] Complex designs, even grayscale photographs could be patterned by varying the laser intensity and irradiation times, as shown in **Figure 8**. As a facile, inexpensive, solid-state method for patterning conductive RGO films, the laser scribing technique holds great promise for engineering low-cost, graphene-based or all-carbon electronic devices via a single-step fabrication process.

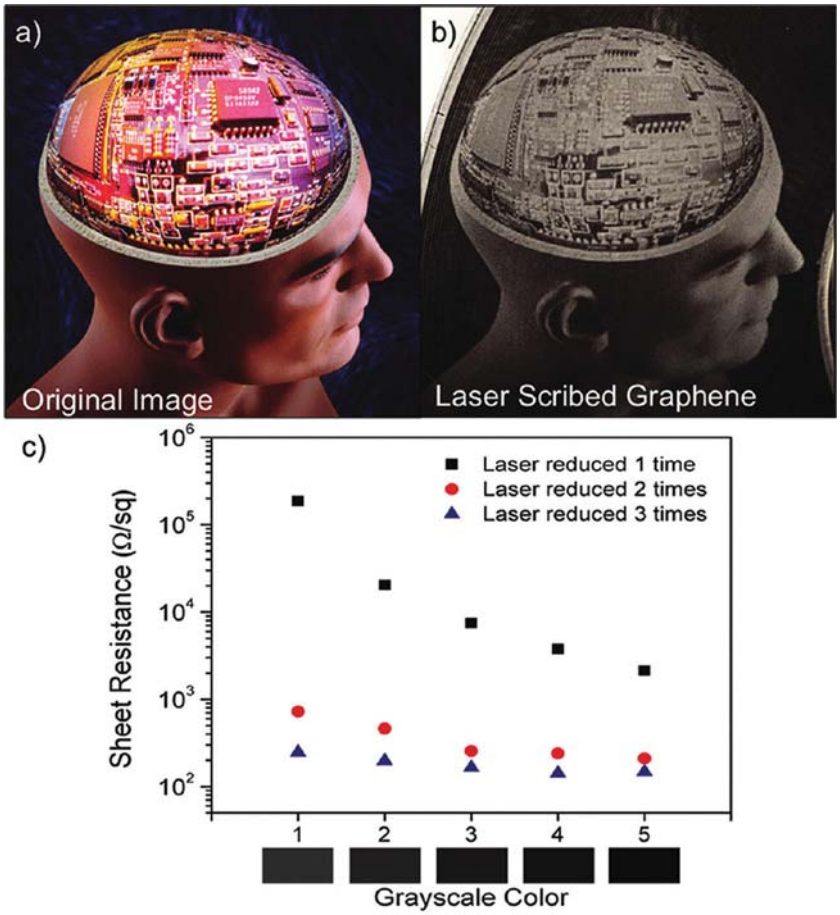

Figure 8. a) A complex colored image of a man's head filled with circuits; b) the same image reproduced on a GO film. The difference in color corresponds to a change in electrical properties. c) A correlation between laser intensity and sheet resistance. Reproduced with permission.[126] Copyright 2012, American Chemical Society.

As compared with electron beam lithography (EBL)[141] and the tip technique,[140] the micropatterns fabricated by DLW still show much lower resolutions, probably due to the light diffraction limit. However, the DLW techniques are still promising, because they permit designable patterning; that means micropatterns of RGO with arbitrary shapes could be easily created according to the computer-designed patterns. More importantly, the resolution, as high as hundreds of nanometers, is high enough for most electronic devices.

3.2. Tunable Reduction Degree

Since the presence of abundant OCGs makes the GO sheets insulating, the reduction of GO is necessary for electronic applications. In comparison with hydrazine treatments and thermal annealing, photoreduction strategies exhibit more refined control over the degree of GO reduction. For example, to realize a tunable reduction degree, more parameters such as the intensity of the light source, irradiation time, light wavelength, scanning time/speed, and photocatalysts could be adjusted. Generally, the reduction degree varies the electrical conductivity of the resultant RGO. In Kaner's work,[126] the sheet resistance of a laser-scribed RGO could be tuned over five orders of magnitude through two ways: i) by direct printing in grayscale color; ii) by controlling the number of times the film is irradiated with the 788 nm infrared laser, as shown in Figure 8c. In addition, Zhang et al. reported the control of the conductivity of RGO films by tuning the power of the femtosecond laser;[87] the higher the laser power, the lower the resistivity. For a comparison of reduction degree among different photoreduction strategies, the properties of RGO (e.g., conductivities and C/O ratios) were summarized in Table 1 and Table 2.

Obviously, in the pursuit of high conductivity, the photoreduction methodology does not show any distinct advantages when compared with thermal and chemical approaches. Nevertheless, the exquisite control over reduction degree makes photoreduction strategies quite unique, since the controllable reduction not only contributes to tunable conductivities, but also varies the amount of residual oxygen species. It is well known that graphene is a zero-bandgap semiconductor;[142] its electronic applications, for instance FETs, have been significantly limited due to the absence of a bandgap. Providing the residual oxygen as a dopant, which can be precisely tuned during the photoreduction of GO, the electronic band structures of RGO could be modulated accordingly.

As a typical example, Zhang et al. investigated the bandgap tailoring of GO by FsLDW both theoretically and experimentally.[143] In their model, GO was simplified with only epoxy radical coverage on the same side of the GO sheet that contains 32 carbon atoms. The variation of the bandgap with 0 to 16 oxygen atoms was in the range of 0–2.74 eV. Since the atomic structure of GO is uncertain for different samples, the first principles calculation only gives the tendency of the bandgap opening with the increase of oxygen content. It is generally accepted that the zero bandgap of graphene comes from the p-bonding band and the p-antibonding band. In the case of RGO, the presence of oxygen would strongly attract electrons from the carbon sheet owing to the larger electronegativity. With the increase of oxygen content, the p electrons of the O atom would bind with the p electrons from graphene, leading to the opening of the bandgap. In addition to the theoretical results, the modulation of the GO bandgap has also been confirmed experimentally, by tuning the reduction degree of GO.

3.3. Control over Surface Wettability

The wettability of solid surfaces has been considered an important property.[144,145] Generally, the surface wettability is governed by two factors: the chemical composition, and the

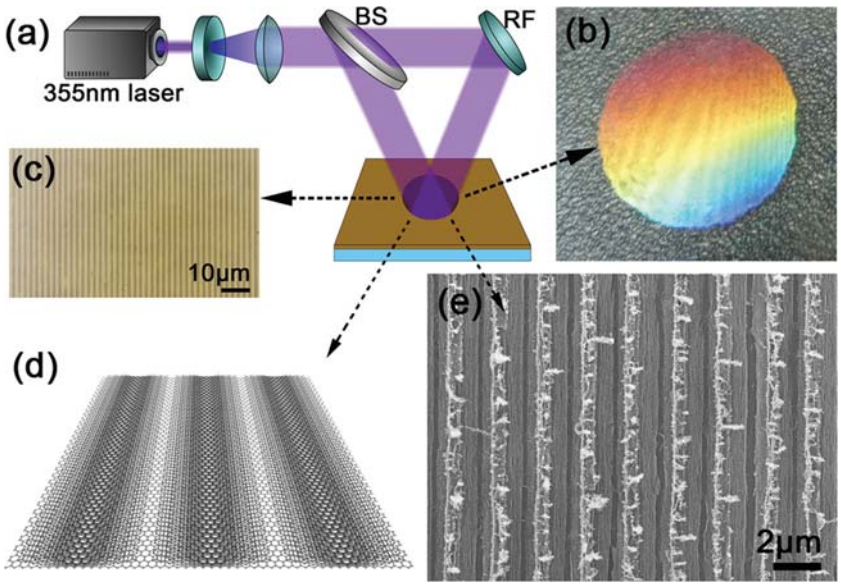

Figure 9. a) A schematic illustration of the two-beam laser interference system for the fabrication of superhydrophobic graphene films. b) A photograph of an as-patterned graphene film. The structural color can be observed by the naked eye. c) An optical microscopic image of the graphene pattern. d) A schematic illustration of the graphene surface after two-beam laser interference treatment. e) An SEM image of the superhydrophobic and iridescent graphene film. Reproduced with permission.[151] Copyright 2012, John Wiley and Sons.

surface topography.[146] By controlling these two factors, artificial surfaces with tunable wettability, represented by adjustable water contact angles (CAs) from 0° to ≈170°, have been readily fabricated.[145] In recent years, triggered by the exceptional properties of graphene, research on the wettability control of graphene surfaces has also been done.[147,148] Theoretically, graphene is predicted to be strongly hydrophobic.[149] However, experimental results show that the water CA of epitaxial graphene is only 92°.[150] Currently, we still cannot directly tune the wettability of pristine graphene by controlling the surface structures; most of the related works deal with GO.

In the case of GO, the surface wettability could be tuned in two ways. One is the tailoring of surface functional groups (e.g., the grating of functional groups), and the other is to control the surface roughness. Photoreduction of GO provides the feasibility of manipulating both of these factors simultaneously. For example, Wang et al. modulated the wettability of RGO in the range of ≈70° (pristine GO) to ≈157° (superhydrophobic surface), by using two-beam laser interference-induced reduction and structuring of a GO film.[151] As shown in **Figure 9**, periodic grating structures of RGO films have been created. Notably, this unique photoreduction method allows the formation of hierarchical micro-nanostructures and the modulation of the chemical composition at the same time.

4. Broad Applications

As inherited from graphene, RGO films prepared by proper reduction of GO possess comparable properties to graphene. In particular, owing to their facile and large-scale preparation, great effort has been devoted to making full use of RGO. Since photoreduction of GO permits exquisite control over both the composition and structures of RGO, it has motivated broad applications beyond that of thermally/chemically reduced GO (**Table 3**).

4.1. Flexible Electronic Devices

In recent years, graphene has emerged as a promising material that could be used for the development of the next generation of electronics due to its ultra-high carrier mobility, high conductivity, transparency, and excellent mechanical strength. However, from the practical point of view, open problems including the mass production, bandgap tailoring, and the compatibility during device fabrication are huge obstacles to graphene-based electronics. As an alternative, GO is promising for engineering low-cost, graphene-based, flexible electronic devices due to the possibility of large-scale preparation and the solvent-processing capability. Nevertheless, conventional thermal and chemical reductions suffer from poor compatibility with device manufacturing techniques, especially for flexible electronic devices that require plastic substrates. In this regard, photoreduction strategies show obvious advantages.[143,152] For instance, Kymakis et al. reported a nonthermal laser reduction of spin-coated GO on flexible substrates over a large area, which could be used as electrodes for organic photovoltaic cells.[153]

On the other hand, the patterning of graphene is necessary for graphene-based electronics regarding their practical use in transparent electrodes,[15] FETs,[143] and sensors.[154] Photoreduction allows non-contact and mask-free patterning of RGO films, which makes the fabrication of graphene-based microdevices much easier, and even permits post-integration of RGO devices without compromising any of their components. Towards the fabrication of an FET device, Guo et al. reported the laser reduction of a RGO channel between two pre-patterned electrodes by FsLDW.[143] Over the whole fabrication process, the RGO channel could be created at desired position in the last step, indicating the unique feature of flexible integration. In addition, Petridis et al. demonstrated the post-fabrication of RGO transistor channels using an excimer pulsed laser, which is compatible with flexible plastic substrates.[152] Using the laser scribing technique, an all-organic flexible set of interdigitiated electrodes have been successfully fabricated.[126] The above-mentioned works reveal that photoreduction holds great promise for the development of RGO-based electronics.

4.2. Graphene-based Sensors

Graphene is a promising sensing material, because every carbon atom on a graphene sheet is a surface atom. Since the gas-sensing mechanism of graphene is generally ascribed to the

Table 3. Typical applications of photoreduced GO and their photoreduction strategies.

Application field	Photoreduction strategy			Ref
	Light sources	Atmosphere (catalysts)	Mechanism[a)]	
Preparation of graphene-like materials	Xenon lamp (300 W)	Solution	PC	[84]
	Hg arc lamp (500 W)	Solution (TiO_2)	PC	[101]
	High-pressure Hg lamp	Solution ($H_3PW_{12}O_{40}$)	PC	[108,109]
Flexible electrodes	Camera flash	Air, N_2	PT	[81]
	Infrared laser (788 nm)	Air	PT	[126,127]
	Femtosecond laser (800 nm)	Air	PT & PC	[153]
FETs	Femtosecond laser (790 nm)	Air	PT & PC	[143]
	Excimer pulsed laser (248 nm)	Vacuum	PT & PC	[152]
	High-pressure Hg lamp	Solution ($H_3PW_{12}O_{40}$)	PC	[108,109]
Gas sensors	Nd:YAG laser (355 nm)	Air	PT & PC	[151,162]
	Hg lamp (500 W)	Solution (WO_3)	PC	[107]
Photovoltaic devices	Xe arc lamp (450 W)	Solution (TiO_2)	PC	[173]
	Xe lamp (300 W)	Air (TiO_2)	PT & PC	[175]
Li-ion batteries	Camera flash	Air	PT	[166,167]
	Xe lamp (1000 W)	Solution (TiO_2)	PC	[185]
Supercapacitors	Infrared laser (788 nm)	Air	PT	[126,127]
	Universal X-660 CO_2 laser	Air	PT	[123]
Photoignition	Camera flash	Air	PT	[82]
Photocatalysis	Xe arc lamp (450 W)	Solution (TiO_2)	PC	[69]
	Xe lamp (500 W)	Solution	PC	[117]
	Hg lamp (110 mW/cm^2)	Solution (ZnO)	PC	[105]
	Xe arc lamp (300 W)	Solution ($BiVO_4$)	PC	[106]
	UV spot lamp (50 W)	Solution	PC	[118]

[a)] PT: Photo-thermal reaction; PC: Photo-chemical reaction.

adsorption/desorption of gaseous molecules that act as electron donors or acceptors,[155] electron transport on graphene is highly sensitive to adsorbed molecules. To date, graphene-based sensors have been successfully developed for the detection of various gases, for instance, toxic aromatic compounds.[156–158] However, problems in the scalable preparation of graphene and its relative weak interaction with guest molecules limit its applications in sensors. As an alternative, the presence of oxygen functional groups on GO not only impart it with solution-processing compatibility but also improve its interactivity with sensing molecules. Despite the fact that a GO film is insulating, its conductivity could be partly restored after appropriate reduction. So far, RGO has been applied to the sensitive detection of various gas molecules such as NO_2, NH_3, CO, Cl_2, H_2, and H_2O.[34,155,159–161]

The photoreduction of GO provides a new opportunity for the controllable removal of OCGs towards the development of sensing devices. Briefly, the photoreduction is unique due to three features: i) tunable reduction (tunable conductivity); ii) controllable OCG content (controllable interactions with sensing molecules); iii) micro-nanostructuring (promotion of adsorption/desorption and mass transfer). Previously, we have reported the fabrication of a humidity-sensing device by two-beam-laser interference treatment of GO.[162] Simultaneous reduction, patterning, and nanostructuring occur after exposing the GO film to interferential laser beams. By tuning the laser power, residual OCGs and film conductivity could be controlled within a certain range, and so could the response/recovery times (**Figure 10**). According to the first principles study, the tunability of response/recovery times could be ascribed to the variety of interactions between H_2O molecules and RGO sheets. Moreover, hierarchical nanostructures generated during laser treatment make the interlayer RGO visible and promote the sensing performance significantly (Figure 10d).

4.3. Li-ion Batteries

Owing to its high electrical conductivity, large specific surface area, mechanical robustness, and excellent stability, graphene is considered a promising candidate for Li-ion battery anodes.[163–165] Generally, for graphene anodes, a high surface area structure is highly desirable because a large contact area between the electrode and electrolyte can lead to good cycling performance and a short path length for Li-transport. From

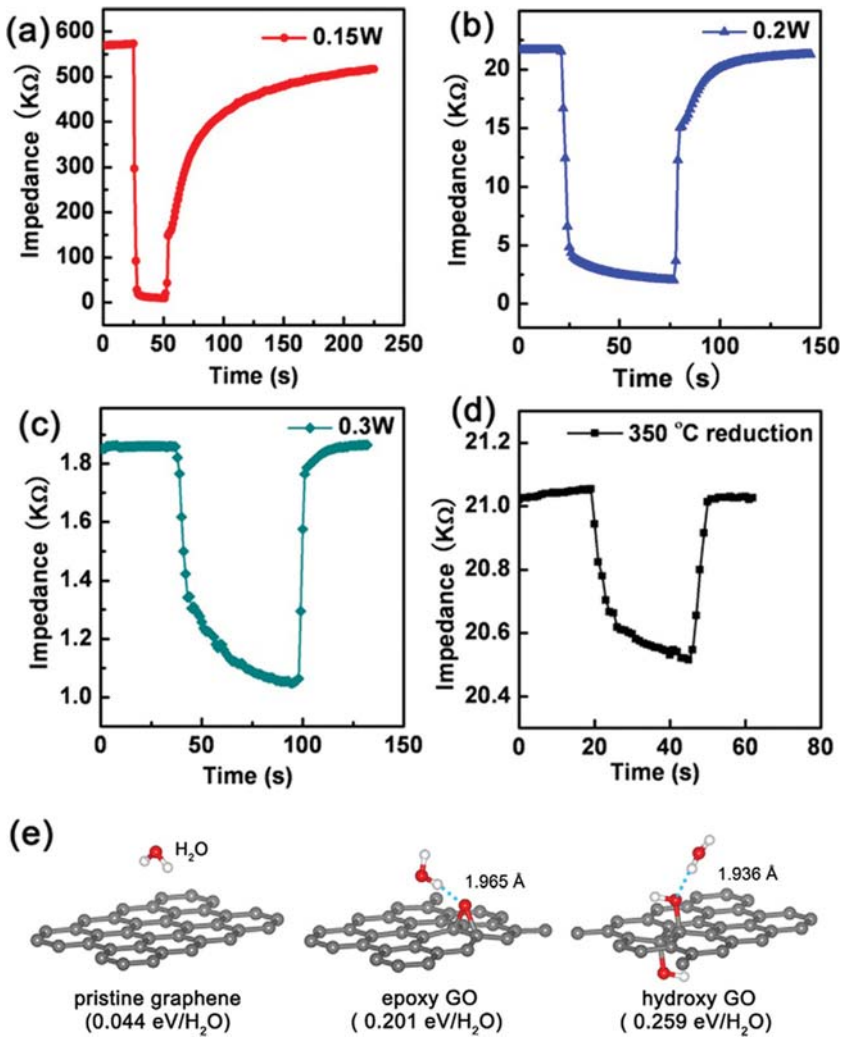

Figure 10. Response and recovery properties of the RGO sensor. GO films were reduced under the laser power of a) 0.15 W, b) 0.2 W, and c) 0.3 W; d) GO was also reduced at 350 °C under the protection of nitrogen for comparison. e) Response/recovery curve of RGO (0.2 W) sensing device for five cycles. The curves were measured between 11% and 95% relative humidity at room temperature. Reproduced with permission.[162] Copyright 2012, Elsevier.

this point of view, the unique flash reduction of GO could provide the opportunity for direct formation of porous graphene anodes for Li-ion batteries.[166] As shown in **Figure 11**, flash-reduced GO anodes exhibit a unique "open-pore" structure due to the drastic expansion, which enables access for Li ions to the underlying graphene sheets and facilitates efficient intercalation kinetics even at ultrafast charge/discharge rates. Moreover, the photothermally reduced GO anodes are structurally robust and display excellent stability and cycling ability.

In a similar manner, Zhao et al. reported the facile fabrication of free-standing, flexible FeF_3–graphene papers as cathodes in high-energy density Li-ion batteries.[167] The flash reduction not only avoids the reaction between FeF_3 and GO at the elevated temperatures, but also provides a porous and electrically conducting graphene support for FeF_3 nanoparticles. The flexible FeF_3–graphene papers show high charge-storage capacity, and good rate and cycling performances, demonstrating great potential for use in flexible and portable Li-ion batteries.

4.4. Supercapacitors

Unlike batteries that store energy via electrochemical reactions, electrochemical capacitors store charge in electrochemical double layers. Despite the fact that electrochemical capacitors show relatively low energy densities as compared with batteries, electrochemical capacitors are still promising in energy storage technologies because they can deliver much higher power densities.[168,169] Graphene is an attractive electrode material due to its distinct advantages including large surface area, mechanical strength, and electrical properties. At present, GO has been widely used in various charge-storage devices, however, as compared with the theoretical value with respect to a single-layer graphene, the specific capacitance, energy density, and power density of GO-based devices are still low because of the van der Waals interaction-induced restacking of RGO sheets during reduction, which significantly reduces the specific surface area of RGO and leads to a relative low capacitance. To overcome this problem, El-Kady et al. reported the production of RGO-based electrochemical capacitors by using the LaserScribing technique.[127] Laser reduction treatmenst can not only avoid the restacking of RGO sheets, but also produce a porous structure (BET surface area: 1520 m^2/g). Using laser-reduced RGO as electrodes, the electrochemical capacitors exhibit both ultrahigh energy density and excellent mechanical stability.

As the LDW technique shows obvious advantages in the manufacturing of micropatterns, Gao et al. reported the DLW fabrication of microsupercapacitors on hydrated GO films.[123] In their work, both in-plane and conventional RGO electrodes with different micropatterns have been design and fabricated by scanning a CO_2 laser on a hydrated GO film. Interestingly, the residual GO region between the patterned RGO electrodes could serve as both an electrolyte and an electrode separator due to the presence of trapped water, which makes it simultaneously a good ionic conductor and an electrical insulator. In this way, a new type of all-carbon, monolithic supercapacitor has been developed by using a single technique. **Figure 12** shows a photograph of an array of concentric circular RGO patterns fabricated on a free-standing hydrated GO film. The SEM image shows that the RGO region is porous due to the generation of various gases, including the product of OCG decomposition and the interlayer water during laser irradiation. The resulting microsupercapacitor devices show very good cyclic stability and energy storage capacities. In particular, the in-plane circular design shows the highest specific capacitance of ≈0.51 mF/cm^2, and a volumetric capacitance of ≈3.1 F/cm^3 (Figure 12d).

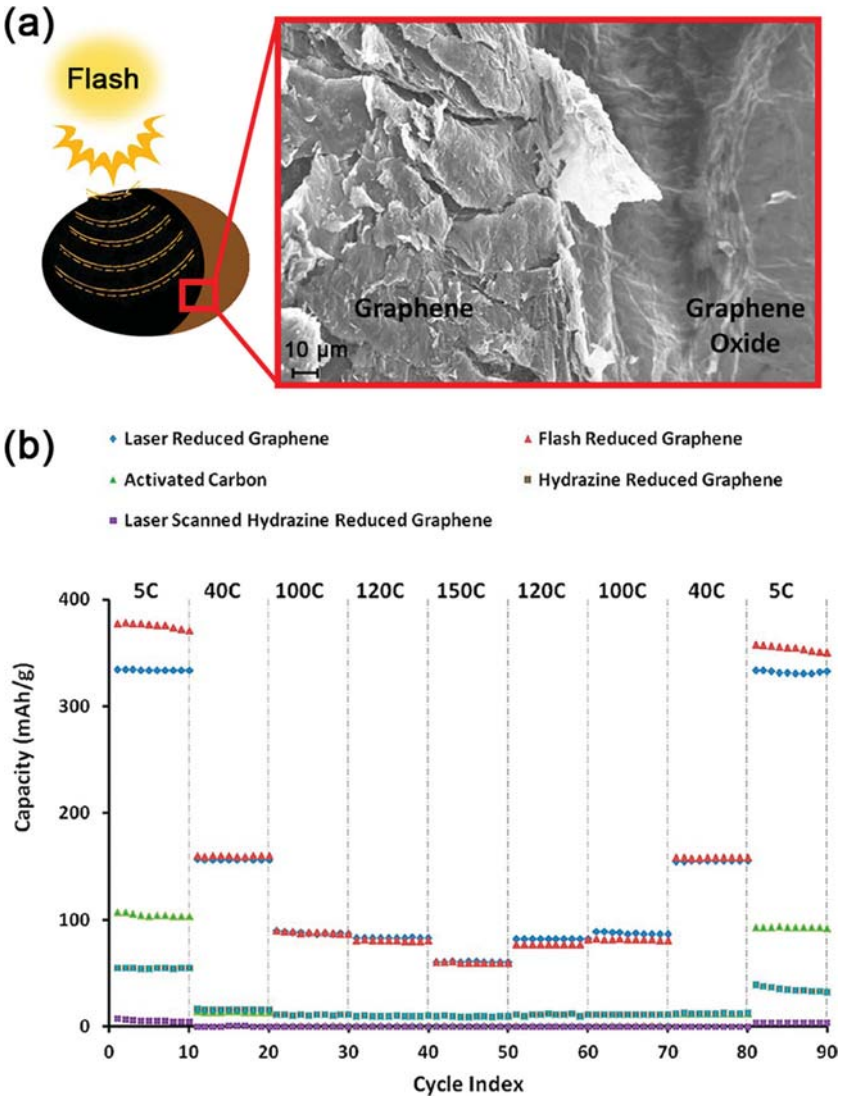

Figure 11. a) Schematic showing the flash reduction of GO and SEM image of the regions containing both flash-reduced GO and GO. b) Performance of laser- and flash-reduced graphene anodes at various C rates, compared to the performance of control samples of activated carbon, hydrazine-reduced graphene, and laser-scanned hydrazine-reduced graphene. The cells were operated for 10 cycles each at different C rates from 5 to 150 C and were then brought back to 5 C in the reverse sequence. Reproduced with permission.[166] Copyright 2012, American Chemical Society.

4.5. Photovoltaic Devices

Dye-sensitized solar cells (DSSCs) have attracted enormous research interest due to their low cost, simple device fabrication process, and moderate energy-conversion efficiency.[170] For DSSCs, the counter electrodes require materials to possess a large specific surface area, high conductivity, chemical stability, and low cost. In recent years, carbonaceous materials including carbon black, carbon nanotubes (CNTs), graphite, and graphene (GR) are emerging as efficient catalysts for use in DSSCs,[171] among which graphene shows distinct advantages such as high electrical conductivity, corrosion resistance, robustness, and a high specific surface area.

Generally, the performance of graphene-based DSSCs can be improved by tuning the C/O ratio or by introducing dopants, since the presence of defects and functional groups determine the electrocatalytic activities.[172] Consequently, photoreduced GO seems promising in DSSCs, because photoreduction permits exquisite control over residual oxygen content, film conductivity, and the introduction of dopants. As an example, Kim et al. reported the photocatalytic reduction of GO and TiO_2 nanocomposites, which were further applied as interfacial layers between a fluorine-doped tin oxide (FTO) layer and a nanocrystalline TiO_2 film to inhibit a back-transport reaction.[173] The photoconversion efficiency was improved from 4.89% to 5.26%, indicating their potential application in photovoltaic devices. An alternating RGO and titania multilayered composite has also been prepared by Manga et al. using layer-by-layer electrostatic deposition and subsequent photocatalytic reduction of GO under UV irradiation.[174] Ultrafast electron transfer and significantly enhanced photoconversion properties were reported based on such hybrid systems. Later, Yao et al. reported the photo-thermal/-catalytic reduction lithography approach for the preparation of poly-diallyldimethylammonium (PDDA)/GO/PDDA/TiO hybrid films on a glass substrate.[175] Their approach allows the fabrication of photoconductive patterns on the hybrid film with the help of a pre-designed shadow mask. The photoconductive response of the as-prepared pattern could be directly tested on the hybrid pattern, which showed a high photocurrent generation and good reversibility.

Furthermore, recent studies show that the use of GO as a buffer layer in organic photovoltaics (OPVs) may significantly enhance its stability. Since the GO or RGO layer may be further reduced under prolonged solar illumination, the improvements of the charge transport characteristics of the OPVs may be attributed to the photoreduction-induced increase in conductivity.[176,177]

4.6. Other Applications

In addition to the above-mentioned applications, GO has also proved its value in other disciplines. For instance, the photocatalytic reduction of GO could be used for the preparation of graphene-doped composite materials that possess enhanced catalytic properties. Li et al. synthesized novel tin(IV) prophyrin (SnPor)/Ag nanoparticles/RGO ternary nanohybrids

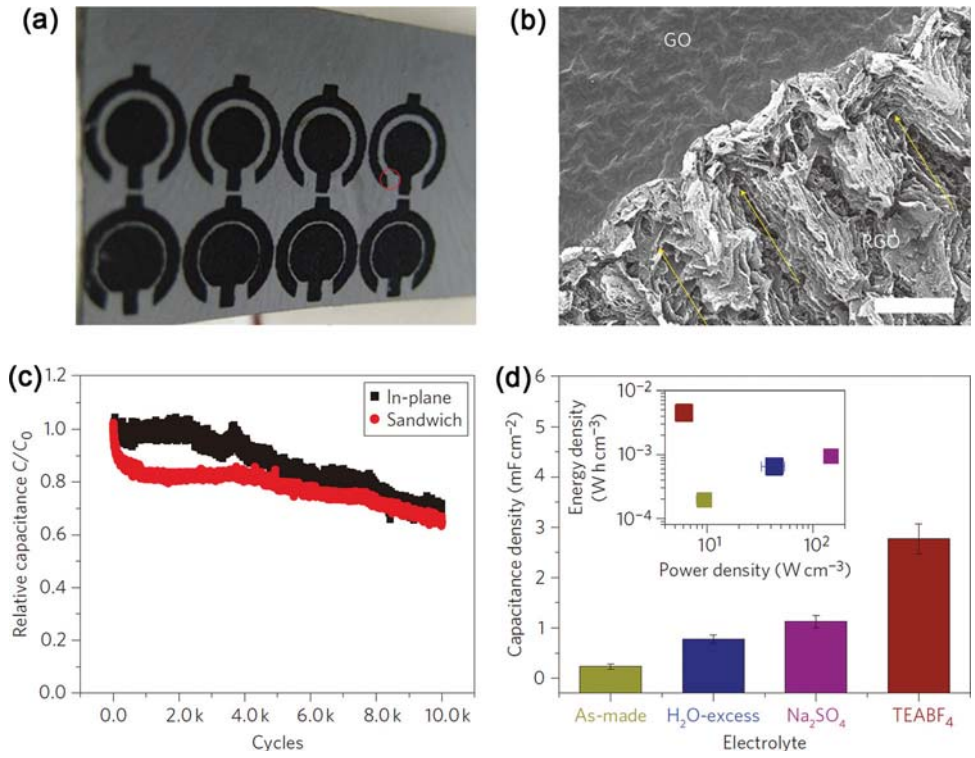

Figure 12. a) Photograph of an array of concentric circular patterns fabricated on a free-standing hydrated GO film; b) SEM image of the interface between GO and RGO (scale bar, 100 mm); c) long cyclability tests of the as-prepared sandwich and concentric circular devices, showing a less than 35% drop in capacitance after 10 000 cycles; d) histogram comparison of area-based capacitance density of a sandwich device as-prepared (dark yellow), with excess DI water (navy), aqueous electrolyte (1.0 M Na_2SO_4, purple), and organic electrolyte (1.0 M TEABF4, burgundy). Inset: volumetric energy density versus power density data of the corresponding devices (shown in the same colours). Reproduced with permission.[123] Copyright 2011, Nature Publishing Group.

via phtotcatalytic reduction of both GO and AgI using SnPor as a photocatalyst.[112] The nanohybrids show good catalytic activities in both the degradation of rhodamine B and the reduction of 4-nitrophenol. Ng et al. reported the preparation of $BiVO_4$/RGO composites by in-situ photoreduction of GO. A remarkable ten-fold enhancement in the photocatalytic water-splitting reaction is observed on the resultant composite under visible illumination, which could be mainly attributed to the longer electron lifetime of excited $BiVO_4$ as the RGO suppressed the charge recombination effectively.[106] Additionally, since the GO and laser-reduced GO can efficiently convert the laser radiation into usable heat,[133] the efficient photothermal energy conversion by GO in solution would also spark enormous research interest in some thermochemical and thermomechanical applications,[178] in addition to the photothermal therapy.[179,180]

Taking advantage of the chemical-free, mask-free, non-contact, and cost-effective features of the laser-reduction strategy, more and more graphene-oriented devices would resort to the use of RGO. Based on the reported results, the potential applications of photoreduced GO were summarized in Table 3. We anticipate that, with the rapid progress of photoreduction methodology, GO may find broad application in the fields of catalysis, optoelectronics, physics, and tissue engineering.

5. Conclusion and Outlook

In this progress report, we have reviewed the photoreduction of GO by various photo-assisted strategies, including i) photothermal reduction; ii) photochemical reduction with and without photocatalysts; iii) laser reduction of GO films and solutions. According to the photon energy threshold of GO reduction (3.2 eV) reported by Smirnov et al.[100] mechanisms for various photoreductions have been proposed and summarized in Tables 1 and 2. However, considering the complex molecular structure of a GO sheet and the broad spectral range of diverse light sources, in most cases, the photoreduction of GO has been implemented through a combination of both photothermal and photochemical processes. In this paper, we categorized the photoreduction strategies according to the major contribution, as reported in the original paper.

Photoreduction of GO imparts unique properties to the resultant RGO. For instance, with the help of Xe irradiation, monolayer RGO sheets could be prepared without the use of any reductive chemicals or stabilizers. By controlling the laser processing parameters, the reduction degree could be tuned continuously, as could the film conductivity. More importantly, the laser reductions allow the production of high-resolution conductive micropatterns on the isolating GO films, which directly contributes to the fabrication and integration of graphene-based

microdevices. Owing to these unique properties, RGO prepared by photoreduction has triggered various applications such as flexible electrodes, FETs, sensors, supercapacitors, Li-ion batteries, photovoltaic devices, and composite photocatalysts. In fact, the use of RGO is not limited to the above-mentioned fields: any graphene-oriented application could use RGO prepared by the photoreduction of GO, since the chemical-free photoreduction processes are more cost-effective and environmentally friendly than conventional thermal/chemical reductions.

Obviously, the final purpose of any reduction treatment is to restore the sp^2 carbon network of GO, just like that of graphene. However, the reported results indicate that it is almost impossible to reach this end. After removing the majority of the OCGs, abundant defects form, which dramatically alters some of the properties of the resultant material, the so-called RGO. Nevertheless, it is not reasonable to ascribe this drawback to the reduction methodologies. Actually, the defects already form during the chemical oxidation process. Although the GO could not be fully recovered to graphene, research efforts have continuously made them closer. Currently, for the topic of "photoreduction of GO", there exist three major challenges. The first is how to reduce the defects. As mentioned above, most of the lattice defects might form during oxidation, so the oxidation degree should be controlled accordingly. In this case, some mildly oxidized GO might be more suitable for the production of low-defect RGO. The photoreduction mechanism should also be paid much attention. Based on an in-depth understanding of the photodynamic mechanism, the photoreduction could be optimized significantly. For instance, theoretical investigation has predicted that GO could be reduced to graphene by femtosecond laser irradiation without damaging the graphene sheet. However, it has not been confirmed experimentally.

The second challenge in the photoreduction of GO, especially for laser reduction, is its relative low efficiency. This mainly depends on the state-of-the-art of the DLW techniques. Once large-scale, parallel, laser-processing systems have been well established, the efficiency of device fabrication would be significantly improved. The third challenge seems more important, that is, how to make full use of the photoreduced GO in various scientific and industrial fields. In addition to the reported devices, the fabrication of other RGO-based devices, for example, organic light-emitting diodes (OLED), electrochromic (EC) devices, or photodiodes, lasers have not been realized using photoreduced GO. Moreover, the application of the photoreduction of GO is not limited to electronics. Recently, both graphene and GO have proved to be biocompatible materials in the field of tissue engineering, and could be used for the culture of human mesenchymal stem cells. Moreover, as laser-scribed RGO has a porous structure and high surface area (≈1500 m^2/g), it might be used as either a highly active catalyst or a catalyst support. Beyond photoreduction, which mainly deals with the removal of OCGs, the phototreatment of GO could also be used for heteroatom doping by using a special atmosphere or in the presence of chemicals. With rapid progress, the photoredution of GO could become a mainstream method for the production of RGO and related materials. We anticipate that the unique photoreduction strategies would trigger broad application of GO in the near future, maybe far beyond its prototype, graphene.

Acknowledgements

This work is supported by the National Basic Research Program of China (973 Program) under Grant No. 2011CB013000, and National Science Foundation of China (Grant nos 90923037, 61008014, 61376123 and 6078048). We also acknowledge the China Postdoctoral Science Foundation no. 20110490156 and the Hong Kong Scholar Program XJ2011014.

Received: July 31, 2013
Revised: April 9, 2013
Published online: October 24, 2013

[1] K. S. Novoselov, A. K. Geim, S. V. Morozov, D. Jiang, Y. Zhang, S. V. Dubonos, I. V. Grigorieva, A. A. Firsov, *Science* **2004**, *306*, 666–669.
[2] A. K. Geim, K. S. Novoselov, *Nat. Mater.* **2007**, *6*, 183–191.
[3] A. K. Geim, *Science* **2009**, *324*, 1530–1534.
[4] X. S. Li, W. W. Cai, J. H. An, S. Kim, J. Nah, D. X. Yang, R. Piner, A. Velamakanni, I. Jung, E. Tutuc, S. K. Banerjee, L. Colombo, R. S. Ruoff, *Science* **2009**, *324*, 1312–1314.
[5] X. Huang, Z. Y. Zeng, Z. X. Fan, J. Q. Liu, H. Zhang, *Adv. Mater.* **2012**, *24*, 5979–6004.
[6] X. Huang, X. Y. Qi, F. Boey, H. Zhang, *Chem. Soc. Rev.* **2012**, *41*, 666–686.
[7] X. Huang, Z. Y. Yin, S. X. Wu, X. Y. Qi, Q. Y. He, Q. C. Zhang, Q. Y. Yan, F. Boey, H. Zhang, *Small* **2011**, *7*, 1876–1902.
[8] Q. Y. He, S. X. Wu, Z. Y. Yin, H. Zhang, *Chem. Sci.* **2012**, *3*, 1764–1772.
[9] S. V. Morozov, K. S. Novoselov, M. I. Katsnelson, F. Schedin, D. C. Elias, J. A. Jaszczak, A. K. Geim, *Phys. Rev. Lett.* **2008**, *100*, 016602.
[10] E. H. Hwang, S. Adam, S. Das Sarma, *Phys. Rev. Lett.* **2007**, *98*, 186806.
[11] X. S. Li, Y. W. Zhu, W. W. Cai, M. Borysiak, B. Y. Han, D. Chen, R. D. Piner, L. Colombo, R. S. Ruoff, *Nano Lett.* **2009**, *9*, 4359–4363.
[12] A. A. Balandin, S. Ghosh, W. Z. Bao, I. Calizo, D. Teweldebrhan, F. Miao, C. N. Lau, *Nano Lett.* **2008**, *8*, 902–907.
[13] C. Lee, X. D. Wei, J. W. Kysar, J. Hone, *Science* **2008**, *321*, 385–388.
[14] Z. S. Wu, W. C. Ren, L. B. Gao, J. P. Zhao, Z. P. Chen, B. L. Liu, D. M. Tang, B. Yu, C. B. Jiang, H. M. Cheng, *ACS Nano* **2009**, *3*, 411–417.
[15] K. S. Kim, Y. Zhao, H. Jang, S. Y. Lee, J. M. Kim, J. H. Ahn, P. Kim, J. Y. Choi, B. H. Hong, *Nature* **2009**, *457*, 706–710.
[16] C. O. Girit, J. C. Meyer, R. Erni, M. D. Rossell, C. Kisielowski, L. Yang, C. H. Park, M. F. Crommie, M. L. Cohen, S. G. Louie, A. Zettl, *Science* **2009**, *323*, 1705–1708.
[17] M. C. Duch, G. R. S. Budinger, Y. T. Liang, S. Soberanes, D. Urich, S. E. Chiarella, L. A. Campochiaro, A. Gonzalez, N. S. Chandel, M. C. Hersam, G. M. Mutlu, *Nano Lett.* **2011**, *11*, 5201–5207.
[18] K. Wang, J. Ruan, H. Song, J. L. Zhang, Y. Wo, S. W. Guo, D. X. Cui, *Nanoscale Res. Lett.* **2011**, *6*, 8.
[19] B. Obradovic, R. Kotlyar, F. Heinz, P. Matagne, T. Rakshit, M. D. Giles, M. A. Stettler, D. E. Nikonov, *Appl. Phys. Lett.* **2006**, *88*, 142102.
[20] X. R. Wang, Y. J. Ouyang, X. L. Li, H. L. Wang, J. Guo, H. J. Dai, *Phys. Rev. Lett.* **2008**, *100*, 206803.
[21] H. G. Sudibya, Q. Y. He, H. Zhang, P. Chen, *ACS Nano* **2011**, *5*, 1990–1994.
[22] Q. Y. He, H. G. Sudibya, Z. Y. Yin, S. X. Wu, H. Li, F. Boey, W. Huang, P. Chen, H. Zhang, *ACS Nano* **2010**, *4*, 3201–3208.
[23] H. X. Chang, G. F. Wang, A. Yang, X. M. Tao, X. Q. Liu, Y. D. Shen, Z. J. Zheng, *Adv. Funct. Mater.* **2010**, *20*, 2893–2902.

[24] D. W. Wang, F. Li, J. P. Zhao, W. C. Ren, Z. G. Chen, J. Tan, Z. S. Wu, I. Gentle, G. Q. Lu, H. M. Cheng, *ACS Nano* **2009**, *3*, 1745–1752.
[25] Z. Y. Yin, S. Y. Sun, T. Salim, S. X. Wu, X. A. Huang, Q. Y. He, Y. M. Lam, H. Zhang, *ACS Nano* **2010**, *4*, 5263–5268.
[26] Q. Y. He, S. X. Wu, S. Gao, X. H. Cao, Z. Y. Yin, H. Li, P. Chen, H. Zhang, *ACS Nano* **2011**, *5*, 5038–5044.
[27] L. G. De Arco, Y. Zhang, C. W. Schlenker, K. Ryu, M. E. Thompson, C. W. Zhou, *ACS Nano* **2010**, *4*, 2865–2873.
[28] H. Park, P. R. Brown, V. Buloyic, J. Kong, *Nano Lett.* **2012**, *12*, 133–140.
[29] R. Won, *Nat. Photonics* **2010**, *4*, 411–411.
[30] Z. Y. Yin, S. X. Wu, X. Z. Zhou, X. Huang, Q. C. Zhang, F. Boey, H. Zhang, *Small* **2010**, *6*, 307–312.
[31] J. L. Song, Z. Y. Yin, Z. J. Yang, P. Amaladass, S. X. Wu, J. Ye, Y. Zhao, W. Q. Deng, H. Zhang, X. W. Liu, *Chem. Eur. J.* **2011**, *17*, 10832–10837.
[32] Y. P. Dan, Y. Lu, N. J. Kybert, Z. T. Luo, A. T. C. Johnson, *Nano Lett.* **2009**, *9*, 1472–1475.
[33] B. Huang, Z. Y. Li, Z. R. Liu, G. Zhou, S. G. Hao, J. Wu, B. L. Gu, W. H. Duan, *J. Phys. Chem. C.* **2008**, *112*, 13442–13446.
[34] J. T. Robinson, F. K. Perkins, E. S. Snow, Z. Q. Wei, P. E. Sheehan, *Nano Lett.* **2008**, *8*, 3137–3140.
[35] S. X. Wu, Q. Y. He, C. L. Tan, Y. D. Wang, H. Zhang, *Small* **2013**, *9*, 1160–1172.
[36] X. H. Cao, Z. Y. Zeng, W. H. Shi, P. R. Yep, Q. Y. Yan, H. Zhang, *Small* **2013**, *9*, 1703–1707.
[37] M. Liu, X. B. Yin, E. Ulin-Avila, B. S. Geng, T. Zentgraf, L. Ju, F. Wang, X. Zhang, *Nature* **2011**, *474*, 64–67.
[38] M. Liu, X. B. Yin, X. Zhang, *Nano Lett.* **2012**, *12*, 1482–1485.
[39] S. Chen, J. W. Zhu, X. D. Wu, Q. F. Han, X. Wang, *ACS Nano* **2010**, *4*, 2822–2830.
[40] S. R. C. Vivekchand, C. S. Rout, K. S. Subrahmanyam, A. Govindaraj, C. N. R. Rao, *J. Chem. Sci.* **2008**, *120*, 9–13.
[41] X. H. Cao, Y. M. Shi, W. H. Shi, G. Lu, X. Huang, Q. Y. Yan, Q. C. Zhang, H. Zhang, *Small* **2011**, *7*, 3163–3168.
[42] H. R. Byon, J. Suntivich, Y. Shao-Horn, *Chem. Mater.* **2011**, *23*, 3421–3428.
[43] C. C. Huang, C. Li, G. Q. Shi, *Energy Environ. Sci.* **2012**, *5*, 8848–8868.
[44] S. X. Wu, Q. Y. He, C. M. Zhou, X. Y. Qi, X. Huang, Z. Y. Yin, Y. H. Yang, H. Zhang, *Nanoscale* **2012**, *4*, 2478–2483.
[45] O. Akhavan, E. Ghaderi, A. Akhavan, *Biomaterials* **2012**, *33*, 8017–8025.
[46] W. C. Lee, C. Lim, H. Shi, L. A. L. Tang, Y. Wang, C. T. Lim, K. P. Loh, *ACS Nano* **2011**, *5*, 7334–7341.
[47] T. R. Nayak, H. Andersen, V. S. Makam, C. Khaw, S. Bae, X. F. Xu, P. L. R. Ee, J. H. Ahn, B. H. Hong, G. Pastorin, B. Ozyilmaz, *ACS Nano* **2011**, *5*, 4670–4678.
[48] A. Martinez, K. Fuse, S. Yamashita, *Appl. Phys. Lett.* **2011**, *99*, 121107.
[49] S. P. Pang, J. M. Englert, H. N. Tsao, Y. Hernandez, A. Hirsch, X. L. Feng, K. Mullen, *Adv. Mater.* **2010**, *22*, 5374–5377.
[50] Z. H. Ni, W. Chen, X. F. Fan, J. L. Kuo, T. Yu, A. T. S. Wee, Z. X. Shen, *Phys. Rev. B* **2008**, *77*, 115416.
[51] T. Ohta, F. El Gabaly, A. Bostwick, J. L. McChesney, K. V. Emtsev, A. K. Schmid, T. Seyller, K. Horn, E. Rotenberg, *New J. Phys.* **2008**, *10*, 023034.
[52] F. Varchon, R. Feng, J. Hass, X. Li, B. N. Nguyen, C. Naud, P. Mallet, J. Y. Veuillen, C. Berger, E. H. Conrad, L. Magaud, *Phys. Rev. Lett.* **2007**, *99*, 126805.
[53] S. J. Chae, F. Gunes, K. K. Kim, E. S. Kim, G. H. Han, S. M. Kim, H. J. Shin, S. M. Yoon, J. Y. Choi, M. H. Park, C. W. Yang, D. Pribat, Y. H. Lee, *Adv. Mater.* **2009**, *21*, 2328–2333.
[54] A. N. Obraztsov, *Nat. Nanotechnol.* **2009**, *4*, 212–213.
[55] A. Reina, X. T. Jia, J. Ho, D. Nezich, H. B. Son, V. Bulovic, M. S. Dresselhaus, J. Kong, *Nano Lett.* **2009**, *9*, 30–35.
[56] Z. P. Chen, W. C. Ren, L. B. Gao, B. L. Liu, S. F. Pei, H. M. Cheng, *Nature Mater.* **2011**, *10*, 424–428.
[57] H. A. Becerril, J. Mao, Z. Liu, R. M. Stoltenberg, Z. Bao, Y. Chen, *ACS Nano* **2008**, *2*, 463–470.
[58] D. A. Dikin, S. Stankovich, E. J. Zimney, R. D. Piner, G. H. B. Dommett, G. Evmenenko, S. T. Nguyen, R. S. Ruoff, *Nature* **2007**, *448*, 457–460.
[59] G. Eda, G. Fanchini, M. Chhowalla, *Nature Nanotechnol.* **2008**, *3*, 270–274.
[60] H. C. Schniepp, J. L. Li, M. J. McAllister, H. Sai, M. Herrera-Alonso, D. H. Adamson, R. K. Prud'homme, R. Car, D. A. Saville, I. A. Aksay, *J. Phys. Chem. B* **2006**, *110*, 8535–8539.
[61] S. Stankovich, D. A. Dikin, R. D. Piner, K. A. Kohlhaas, A. Kleinhammes, Y. Jia, Y. Wu, S. T. Nguyen, R. S. Ruoff, *Carbon* **2007**, *45*, 1558–1565.
[62] C. L. Tan, X. Huang, H. Zhang, *Mater. Today* **2013**, *16*, 29–36.
[63] X. Huang, S. Z. Li, Y. Z. Huang, S. X. Wu, X. Z. Zhou, C. L. Gan, F. Boey, C. A. Mirkin, H. Zhang, *Nat. Commun.* **2011**, *2*, 292.
[64] X. Huang, S. Z. Li, S. X. Wu, Y. Z. Huang, F. Boey, C. L. Gan, H. Zhang, *Adv. Mater.* **2012**, *24*, 979–983.
[65] X. Huang, H. Li, S. Z. Li, S. X. Wu, F. Boey, J. Ma, H. Zhang, *Angew. Chem. Int. Ed.* **2011**, *50*, 12245–12248.
[66] X. Huang, X. Z. Zhou, S. X. Wu, Y. Y. Wei, X. Y. Qi, J. Zhang, F. Boey, H. Zhang, *Small* **2010**, *6*, 513–516.
[67] C. Nethravathi, M. Rajamathi, *Carbon* **2008**, *46*, 1994–1998.
[68] G. K. Ramesha, S. Sampath, *J. Phys. Chem. C* **2009**, *113*, 7985–7989.
[69] G. Williams, B. Seger, P. V. Kamat, *ACS Nano* **2008**, *2*, 1487–1491.
[70] J. L. Zhang, H. J. Yang, G. X. Shen, P. Cheng, J. Y. Zhang, S. W. Guo, *Chem. Commun.* **2010**, *46*, 1112–1114.
[71] Y. W. Zhu, S. Murali, M. D. Stoller, A. Velamakanni, R. D. Piner, R. S. Ruoff, *Carbon* **2010**, *48*, 2118–2122.
[72] W. Gao, L. B. Alemany, L. J. Ci, P. M. Ajayan, *Nat. Chem.* **2009**, *1*, 403–408.
[73] H. J. Shin, K. K. Kim, A. Benayad, S. M. Yoon, H. K. Park, I. S. Jung, M. H. Jin, H. K. Jeong, J. M. Kim, J. Y. Choi, Y. H. Lee, *Adv. Funct. Mater.* **2009**, *19*, 1987–1992.
[74] H. L. Li, C. Bubeck, *Macromol. Res.* **2013**, *21*, 290–297.
[75] S. F. Pei, H. M. Cheng, *Carbon* **2012**, *50*, 3210–3228.
[76] X. F. Gao, J. Jang, S. Nagase, *J.Phys. Chem. C.* **2010**, *114*, 832–842.
[77] R. Larciprete, S. Fabris, T. Sun, P. Lacovig, A. Baraldi, S. Lizzit, *J. Am. Chem. Soc.* **2011**, *133*, 17315–17321.
[78] I. K. Moon, J. Lee, H. Lee, *Chem. Commun.* **2011**, *47*, 9681–9683.
[79] S. Park, J. An, J. R. Potts, A. Velamakanni, S. Murali, R. S. Ruoff, *Carbon* **2011**, *49*, 3019–3023.
[80] L. Song, F. Khoerunnisa, W. Gao, W. H. Dou, T. Hayashi, K. Kaneko, M. Endo, P. M. Ajayan, *Carbon* **2013**, *52*, 608–612.
[81] L. J. Cote, R. Cruz-Silva, J. X. Huang, *J. Am. Chem. Soc.* **2009**, *131*, 11027–11032.
[82] S. Gilje, S. Dubin, A. Badakhshan, J. Farrar, S. A. Danczyk, R. B. Kaner, *Adv. Mater.* **2010**, *22*, 419–423.
[83] M. Koinuma, C. Ogata, Y. Kamei, K. Hatakeyama, H. Tateishi, Y. Watanabe, T. Taniguchi, K. Gezuhara, S. Hayami, A. Funatsu, M. Sakata, Y. Kuwahara, S. Kurihara, Y. Matsumoto, *J. Phys. Chem. C* **2012**, *116*, 19822–19827.
[84] X. H. Li, J. S. Chen, X. C. Wang, M. E. Schuster, R. Schlogl, M. Antonietti, *ChemSusChem* **2012**, *5*, 642–646.
[85] A. L. Stroyuk, N. S. Andryushina, N. D. Shcherban, V. G. Il'in, V. S. Efanov, I. B. Yanchuk, S. Y. Kuchmii, V. D. Pokhodenko, *Theor. Exp. Chem.* **2012**, *48*, 2–13.
[86] D. A. Sokolov, K. R. Shepperd, T. M. Orlando, *J. Phys. Chem. Lett.* **2010**, *1*, 2633–2636.
[87] Y. L. Zhang, L. Guo, S. Wei, Y. Y. He, H. Xia, Q. D. Chen, H. B. Sun, F. S. Xiao, *Nano Today* **2010**, *5*, 15–20.

[88] Y. Zhou, Q. L. Bao, B. Varghese, L. A. L. Tang, C. K. Tan, C. H. Sow, K. P. Loh, *Adv. Mater.* **2010**, *22*, 67–71.
[89] B. C. Brodie, *Philoso. T. R. Soc.* **1859**, *149*, 249.
[90] W. S. Hummers, R. E. Offeman, *J. Am. Chem. Soc.* **1958**, *80*, 1339.
[91] H. He, J. Klinowski, M. Forster, A. Lerf, *Chem. Phys. Lett.* **1998**, *287*, 53–56.
[92] M. Cheng, R. Yang, L. C. Zhang, Z. W. Shi, W. Yang, D. M. Wang, G. B. Xie, D. X. Shi, G. Y. Zhang, *Carbon* **2012**, *50*, 2581–2587.
[93] S. Eigler, C. Dotzer, A. Hirsch, *Carbon* **2012**, *50*, 3666–3673.
[94] Y. Gao, H. L. Yip, K. S. Chen, K. M. O'Malley, O. Acton, Y. Sun, G. Ting, H. Z. Chen, A. K. Y. Jen, *Adv. Mater.* **2011**, *23*, 1903–1908.
[95] S. K. Hong, J. E. Kim, S. O. Kim, S. Y. Choi, B. J. Cho, *IEEE Electr. Device Lett.* **2010**, *31*, 1005–1007.
[96] J. Q. Liu, Z. Y. Yin, X. H. Cao, F. Zhao, A. P. Lin, L. H. Xie, Q. L. Fan, F. Boey, H. Zhang, W. Huang, *ACS Nano* **2010**, *4*, 3987–3992.
[97] G. H. Lu, S. Park, K. H. Yu, R. S. Ruoff, L. E. Ocola, D. Rosenmann, J. H. Chen, *ACS Nano* **2011**, *5*, 1154–1164.
[98] Y. X. Lu, H. Kong, F. Wen, S. C. Zhang, X. R. Zhang, *Chem. Commun.* **2013**, *49*, 81–83.
[99] D. Krishnan, F. Kim, J. Y. Luo, R. Cruz-Silva, L. J. Cote, H. D. Jang, J. X. Huang, *Nano Today* **2012**, *7*, 137–152.
[100] V. A. Smirnov, A. A. Arbuzov, Y. M. Shul'ga, S. A. Baskakov, V. M. Martynenko, V. E. Muradyan, E. I. Kresova, *High Energy Chem.* **2011**, *45*, 57–61.
[101] J. W. Jang, S. Cho, G. H. Moon, K. Ihm, J. Y. Kim, D. H. Youn, S. Lee, Y. H. Lee, W. Choi, K. H. Lee, J. S. Lee, *Chem. Eur. J.* **2012**, *18*, 2762–2767.
[102] H. B. Li, W. Zhang, L. D. Zou, L. K. Pan, Z. Sun, *J. Mater. Res.* **2011**, *26*, 970–973.
[103] P. Wang, J. Wang, T. S. Ming, X. F. Wang, H. G. Yu, J. G. Yu, Y. G. Wang, M. Lei, *ACS Appl. Mater. Interf.* **2013**, *5*, 2924–2929.
[104] O. Akhavan, M. Abdolahad, A. Esfandiar, M. Mohatashamifar, *J. Phys. Chem. C.* **2010**, *114*, 12955–12959.
[105] O. Akhavan, *Carbon* **2011**, *49*, 11–18.
[106] Y. H. Ng, A. Iwase, A. Kudo, R. Amal, *J. Phys. Chem. Lett.* **2010**, *1*, 2607–2612.
[107] J. W. Qin, M. H. Cao, N. Li, C. W. Hu, *J. Mater. Chem.* **2011**, *21*, 17167–17174.
[108] H. Li, S. Pang, X. Feng, K. Mullen, C. Bubeck, *Chem. Commun.* **2010**, *46*, 6243–6245.
[109] H. L. Li, S. P. Pang, S. Wu, X. L. Feng, K. Mullen, C. Bubeck, *J. Am. Chem. Soc.* **2011**, *133*, 9423–9429.
[110] D. M. Jang, Y. Myung, H. S. Im, Y. S. Seo, Y. J. Cho, C. W. Lee, J. Park, A. Y. Jee, M. Lee, *Chem. Commun.* **2012**, *48*, 696–698.
[111] M. A. Khaderbad, V. Tjoa, T. Z. Oo, J. Wei, M. Sheri, R. Mangalampalli, V. R. Rao, S. G. Mhaisalkar, N. Mathews, *RSC Advances* **2012**, *2*, 4120–4124.
[112] H. Y. Li, Y. W. Zhang, G. H. Chang, S. Liu, J. Q. Tian, Y. L. Luo, A. M. Asiri, A. O. Al-Youbi, X. P. Sun, *ChemPlusChem* **2012**, *77*, 545–550.
[113] H. H. Zhang, Q. Liu, K. Feng, B. Chen, C. H. Tung, L. Z. Wu, *Langmuir* **2012**, *28*, 8224–8229.
[114] T. S. Wu, S. Liu, Y. L. Luo, W. B. Lu, L. Wang, X. P. Sun, *Nanoscale* **2011**, *3*, 2142–2144.
[115] Y. Matsumoto, M. Koinuma, S. Y. Kim, Y. Watanabe, T. Taniguchi, K. Hatakeyama, H. Tateishi, S. Ida, *ACS Appl. Mater. Interf.* **2010**, *2*, 3461–3466.
[116] D. Li, M. B. Muller, S. Gilje, R. B. Kaner, G. G. Wallace, *Nat. Nanotechnol.* **2008**, *3*, 101–105.
[117] Y. Matsumoto, M. Koinuma, S. Ida, S. Hayami, T. Taniguchi, K. Hatakeyama, H. Tateishi, Y. Watanabe, S. Amano, *J. Phys. Chem. C* **2011**, *115*, 19280–19286.
[118] L. Guardia, S. Villar-Rodil, J. I. Paredes, R. Rozada, A. Martinez-Alonso, J. M. D. Tascon, *Carbon.* **2012**, *50*, 1014–1024.
[119] T. S. Wu, S. Liu, H. L. Li, L. Wang, X. P. Sun, *J. Nanosci. Nanotechnol.* **2011**, *11*, 10078–10081.
[120] T. H. Ji, Y. Y. Hua, M. Sun, N. Ma, *Carbon* **2013**, *54*, 412–418.
[121] Y. L. Zhang, Q. D. Chen, H. Xia, H. B. Sun, *Nano Today* **2010**, *5*, 435–448.
[122] Y. Zhou, K. P. Loh, *Adv. Mater.* **2010**, *22*, 3615–3620.
[123] W. Gao, N. Singh, L. Song, Z. Liu, A. L. M. Reddy, L. J. Ci, R. Vajtai, Q. Zhang, B. Q. Wei, P. M. Ajayan, *Nat. Nanotechnol.* **2011**, *6*, 496–500.
[124] Y. Tao, B. Varghese, M. Jaiswal, S. Wang, Z. Zhang, B. Oezyilmaz, K. P. Loh, E. S. Tok, C. H. Sow, *Appl. Phys. A.* **2012**, *106*, 523–531.
[125] H. F. Teoh, Y. Tao, E. S. Tok, G. W. Ho, C. H. Sow, *J. Appl. Phys.* **2012**, 112.
[126] V. Strong, S. Dubin, M. F. El-Kady, A. Lech, Y. Wang, B. H. Weiller, R. B. Kaner, *ACS Nano* **2012**, *6*, 1395–1403.
[127] M. F. El-Kady, V. Strong, S. Dubin, R. B. Kaner, *Science* **2012**, *335*, 1326–1330.
[128] H. Zhang, Y. Miyamoto, *Phys. Rev. B* **2012**, 85.
[129] C. Casiraghi, S. Pisana, K. S. Novoselov, A. K. Geim, A. C. Ferrari, *Appl. Phys. Lett.* **2007**, 91.
[130] S. Prezioso, M. Perrozzi, M. Donarelli, F. Bisti, S. Santucci, L. Palladino, M. Nardone, E. Treossi, V. Palermo, L. Ottaviano, *Langmuir* **2012**, *28*, 5489–5495.
[131] R. Trusovas, K. Ratautas, G. Raciukaitis, J. Barkauskas, I. Stankeviciene, G. Niaura, R. Mazeikiene, *Carbon* **2013**, *52*, 574–582.
[132] D. A. Sokolov, C. M. Rouleau, D. B. Geohegan, T. M. Orlando, *Carbon* **2013**, *53*, 81–89.
[133] V. Abdelsayed, S. Moussa, H. M. Hassan, H. S. Aluri, M. M. Collinson, M. S. El-Shall, *J. Phys. Chem. Lett.* **2010**, *1*, 2804–2809.
[134] Z. B. Liu, X. Zhao, X. L. Zhang, X. Q. Yan, Y. P. Wu, Y. S. Chen, J. G. Tian, *J. Phys. Chem. Lett.* **2011**, *2*, 1972–1977.
[135] M. Feng, H. B. Zhan, Y. Chen, *Appl. Phys. Lett.* **2010**, 96.
[136] L. Huang, Y. Liu, L. C. Ji, Y. Q. Xie, T. Wang, W. Z. Shi, *Carbon* **2011**, *49*, 2431–2436.
[137] H. W. Chang, Y. C. Tsai, C. W. Cheng, C. Y. Lin, P. H. Wu, *Electrochem. Commun.* **2012**, *23*, 37–40.
[138] D. C. Wei, Y. Q. Liu, *Adv. Mater.* **2010**, *22*, 3225–3241.
[139] J. Feng, W. B. Li, X. F. Qian, J. S. Qi, L. Qi, J. Li, *Nanoscale* **2012**, *4*, 4883–4899.
[140] Z. Q. Wei, D. B. Wang, S. Kim, S. Y. Kim, Y. K. Hu, M. K. Yakes, A. R. Laracuente, Z. T. Dai, S. R. Marder, C. Berger, W. P. King, W. A. de Heer, P. E. Sheehan, E. Riedo, *Science* **2010**, *328*, 1373–1376.
[141] M. Y. Han, B. Ozyilmaz, Y. B. Zhang, P. Kim, *Phys. Rev. Lett.* **2007**, 98.
[142] I. Meric, M. Y. Han, A. F. Young, B. Ozyilmaz, P. Kim, K. L. Shepard, *Nat. Nanotechnol.* **2008**, *3*, 654–659.
[143] L. Guo, R. Q. Shao, Y. L. Zhang, H. B. Jiang, X. B. Li, S. Y. Xie, B. B. Xu, Q. D. Chen, J. F. Song, H. B. Sun, *J. Phys. Chem. C* **2012**, *116*, 3594–3599.
[144] K. S. Liu, L. Jiang, *Nano Today* **2011**, *6*, 155–175.
[145] Y. L. Zhang, H. Xia, E. Kim, H. B. Sun, *Soft Matter* **2012**, *8*, 11217–11231.
[146] K. S. Liu, X. Yao, L. Jiang, *Chem. Soc. Rev.* **2010**, *39*, 3240–3255.
[147] J. Rafiee, M. A. Rafiee, Z. Z. Yu, N. Koratkar, *Adv. Mater.* **2010**, *22*, 2151–2154.
[148] Y. L. Zhang, Q. D. Chen, Z. Jin, E. Kim, H. B. Sun, *Nanoscale* **2012**, *4*, 4858–4869.
[149] O. Leenaerts, B. Partoens, F. M. Peeters, *Phys. Rev. B* **2009**, *79*, 235440.
[150] Y. J. Shin, Y. Y. Wang, H. Huang, G. Kalon, A. T. S. Wee, Z. X. Shen, C. S. Bhatia, H. Yang, *Langmuir* **2010**, *26*, 3798–3802.

[151] J. N. Wang, R. Q. Shao, Y. L. Zhang, L. Guo, H. B. Jiang, D. X. Lu, H. B. Sun, *Chem. Asian J.* **2012**, *7*, 301–304.
[152] C. Petridis, Y. H. Lin, K. Savva, G. Eda, E. Kymakis, T. D. Anthopoulos, E. Stratakis, *Appl. Phys. Lett.* **2013**, *102*, 093115.
[153] E. Kymakis, K. Savva, M. M. Stylianakis, C. Fotakis, E. Stratakis, *Adv. Funct. Mater.* **2013**, *23*, 2742–2749.
[154] L. Huang, Y. Huang, J. J. Liang, X. J. Wan, Y. S. Chen, *Nano Res.* **2011**, *4*, 675–684.
[155] I. Jung, D. Dikin, S. Park, W. Cai, S. L. Mielke, R. S. Ruoff, *J. Phys. Chem. C* **2008**, *112*, 20264–20268.
[156] F. Schedin, A. K. Geim, S. V. Morozov, E. W. Hill, P. Blake, M. I. Katsnelson, K. S. Novoselov, *Nat. Mater.* **2007**, *6*, 652–655.
[157] Q. M. Ji, S. B. Yoon, J. P. Hill, A. Vinu, J. S. Yu, K. Ariga, *J. Am. Chem. Soc.* **2009**, *131*, 4220–4221.
[158] K. Ariga, A. Vinu, Q. M. Ji, O. Ohmori, J. P. Hill, S. Acharya, J. Koike, S. Shiratori, *Angew. Chem. Int. Ed.* **2008**, *47*, 7254–7257.
[159] V. Dua, S. P. Surwade, S. Ammu, S. R. Agnihotra, S. Jain, K. E. Roberts, S. Park, R. S. Ruoff, S. K. Manohar, *Angew. Chem. Int. Ed.* **2010**, *49*, 2154–2157.
[160] G. H. Lu, L. E. Ocola, J. H. Chen, *Appl. Phys. Lett.* **2009**, *94*, 083111.
[161] J. D. Fowler, M. J. Allen, V. C. Tung, Y. Yang, R. B. Kaner, B. H. Weiller, *ACS Nano* **2009**, *3*, 301–306.
[162] L. Guo, H. B. Jiang, R. Q. Shao, Y. L. Zhang, S. Y. Xie, J. N. Wang, X. B. Li, F. Jiang, Q. D. Chen, T. Zhang, H. B. Sun, *Carbon* **2012**, *50*, 1667–1673.
[163] X. Zhao, C. M. Hayner, M. C. Kung, H. H. Kung, *Adv. Energy Mater.* **2011**, *1*, 1079–1084.
[164] X. Zhao, C. M. Hayner, M. C. Kung, H. H. Kung, *ACS Nano* **2011**, *5*, 8739–8749.
[165] S. Y. Yin, Y. Y. Zhang, J. H. Kong, C. J. Zou, C. M. Li, X. H. Lu, J. Ma, F. Y. C. Boey, X. D. Chen, *ACS Nano* **2011**, *5*, 3831–3838.
[166] R. Mukherjee, A. V. Thomas, A. Krishnamurthy, N. Koratkar, *ACS Nano* **2012**, *6*, 7867–7878.
[167] X. Zhao, C. M. Hayner, M. C. Kung, H. H. Kung, *Chem. Commun.* **2012**, *48*, 9909–9911.
[168] C. Liu, F. Li, L. P. Ma, H. M. Cheng, *Adv. Mater.* **2010**, *22*, E28-E62.
[169] D. S. Su, R. Schlogl, *ChemSusChem* **2010**, *3*, 136–168.
[170] B. E. Hardin, H. J. Snaith, M. D. McGehee, *Nat. Photonics.* **2012**, *6*, 162–169.
[171] L. J. Brennan, M. T. Byrne, M. Bari, Y. K. Gun'ko, *Adv. Energy Mater.* **2011**, *1*, 472–485.
[172] H. Wang, Y. H. Hu, *Energy Environ. Sci.* **2012**, *5*, 8182–8188.
[173] S. R. Kim, M. K. Parvez, M. Chhowalla, *Chem. Phys. Lett.* **2009**, *483*, 124–127.
[174] K. K. Manga, Y. Zhou, Y. L. Yan, K. P. Loh, *Adv. Funct. Mater.* **2009**, *19*, 3638–3643.
[175] H. B. Yao, L. H. Wu, C. H. Cui, H. Y. Fang, S. H. Yu, *J. Mater. Chem.* **2010**, *20*, 5190–5195.
[176] E. Stratakis, M. M. Stylianakis, E. Koudoumas, E. Kymakis, *Nanoscale* **2013**, *5*, 4144–4150.
[177] J. M. Yun, J. S. Yeo, J. Kim, H. G. Jeong, D. Y. Kim, Y. J. Noh, S. S. Kim, B. C. Ku, S. I. Na, *Adv. Mater.* **2011**, *23*, 4923–4928.
[178] J. R. Potts, S. H. Lee, T. M. Alam, J. An, M. D. Stoller, R. D. Piner, R. S. Ruoff, *Carbon* **2011**, *49*, 2615–2623.
[179] S. H. Hu, Y. W. Chen, W. T. Hung, I. W. Chen, S. Y. Chen, *Adv. Mater.* **2012**, *24*, 1748–1754.
[180] K. Yang, J. M. Wan, S. Zhang, B. Tian, Y. J. Zhang, Z. Liu, *Biomaterials* **2012**, *33*, 2206–2214.
[181] V. Eswaraiah, S. S. J. Aravind, S. Ramaprabhu, *J. Mater. Chem.* **2011**, *21*, 6800–6803.
[182] Y. H. Ding, P. Zhang, Q. Zhuo, H. M. Ren, Z. M. Yang, Y. Jiang, *Nanotechnology* **2011**, *22*, 215601.
[183] P. Fabbri, L. Valentini, S. B. Bon, D. Foix, L. Pasquali, M. Montecchi, M. Sangermano, *Polymer* **2012**, *53*, 6039–6044.
[184] H. C. Huang, C. W. Huang, C. T. Hsieh, P. L. Kuo, J. M. Ting, H. S. Teng, *J. Phys. Chem. C.* **2011**, *115*, 20689–20695.
[185] J. X. Qiu, P. Zhang, M. Ling, S. Li, P. R. Liu, H. J. Zhao, S. Q. Zhang, *Acs Appl. Mater. Interf.* **2012**, *4*, 3636–3642.